MAPPING OCEAN NOISE:

MODELLING CUMULATIVE ACOUSTIC ENERGY FROM SHIPPING IN BRITISH COLUMBIA TO INFORM MARINE SPATIAL PLANNING

Report for

World Wildlife Fund Canada

Attn. Hussein Alidina

409 Granville St., Suite 1588, Vancouver, BC V6C 1T2 Canada
Ph. +1-416 – 489 8800; HAlidina@WWFCanada.org

by

Dr. Christine Erbe

Centre for Marine Science & Technology

Curtin University
GPO Box U 1987, Perth, Western Australia 6845
Ph. +61-8-9266 7380; C.Erbe@curtin.edu.au

Project CMST 1029 Report R2012-10

20 February 2012

Suggested citation:

Erbe, C., MacGillivray, A., and Williams, R. 2012. Mapping Ocean Noise: Modelling Cumulative Acoustic Energy from Shipping in British Columbia to Inform Marine Spatial Planning. Report submitted to WWF Canada by Curtin University, Australia.

Affiliations:

Dr Christine Erbe
Director, Centre for Marine Science & Technology
Curtin University
GPO Box U1987, Perth, Western Australia 6845

Mr Alexander MacGillivray
JASCO Applied Sciences
2101 – 4464 Markham St.
Victoria, British Columbia
V8Z 7X8 Canada

Dr Rob Williams
Sea Mammal Research Unit, Scottish Oceans Institute
University of St Andrews, St Andrews, Fife, KY16 8LB, Scottland;
and Oceans Initiative, Pearse Island, Box 193, Alert Bay
British Columbia, V0N 1A0 Canada

Executive Summary

Sound propagates extremely well through water. Many marine animals have evolved mechanisms to exploit this property, to the extent that, for many species, sound is the primary modality for communication and sensing. In recent decades, the extent and intensity of anthropogenic noise sources have been growing. Commercial shipping is one of the most important global contributors to anthropogenic ambient noise levels. Shipping noise can be considered a chronic, habitat-level stressor to marine wildlife. A variety of point-source and area-based management tools could be used to assess and mitigate impacts, but the ability to include ocean noise as a stressor in marine spatial planning efforts hinges on a good assessment of noise levels at regional or ocean-basin scales and temporal scales that integrate noise exposure over ecologically meaningful periods, such as a whale's feeding season or a year. We developed one such prediction of shipping noise levels throughout the Exclusive Economic Zone of Canada's Pacific waters.

Dalhousie University, within the framework of an oil-spill response project, collated a database of shipping routes and vessel traffic logs for the Canadian Pacific coast. A matrix of vessel hours within a 5 km x 5 km geographic grid was made available for this noise-mapping project. The database allowed the grouping of vessels by size. Based on a review of the literature, our own recordings and published ship noise models, we assigned source spectrum levels to each of five vessel classes. Transmission loss was modelled accounting for geometric spreading (a combination of spherical and cylindrical spreading) and volume absorption. Received levels were computed by integrating over all vessels within a 100 km radius, and by integrating over time. The result was a map of cumulative underwater acoustic energy from shipping over 12 months in the year of 2008.

The noise map showed highest levels within the Straits of Georgia and Juan de Fuca, and Puget Sound, due to the location of the ports of Vancouver and Seattle. A secondary noise “hot spot” was identified near the port of Prince Rupert. The maximum modelled sound exposure level was 215 dB re 1 μPa^2s near Seattle. Many mainland fjords were predicted to have low sound exposure levels, and the potential for these to serve as acoustic refuges warrants closer attention in the form of fine-scale modelling and focused field data collection.

A sensitivity analysis was performed to determine the uncertainty of the noise map as a function of variability of bathymetry, seafloor geology and water parameters. Bathymetry was the main factor affecting received levels at the low frequencies (< 200 Hz) of maximum ship energy. During the winter months, a mild surface duct existed in the water column reducing sound propagation interactions with the seafloor and allowing energy at higher frequencies to travel over long ranges with little loss. During the summer months, the water was downward refracting increasing seafloor interactions and significantly reducing long-range propagation of sound at higher

frequencies. Soft sediment absorbed more energy than hard hence more reflective sediment.

Errors in transmission loss were further assessed by comparison to field measurements off northern British Columbia. Errors in source level were estimated from the literature. The laws of error propagation were applied to estimate the standard deviation of the modelled received levels. The standard deviation of the cumulative sound exposure level in the cells of highest ship traffic was estimated to be 9 dB. Errors in cumulative received levels in cells farther from the shipping lanes were estimated higher in inshore water due to the variability in the hydro- and geoacoustic environment.

We present these maps as a first approximation of predicted noise levels in BC waters, with an associated level of uncertainty. The results predict persistent, large-scale spatial variability in cumulative noise energy, although fine-scale modelling is needed to resolve the narrow straits and fjords. We see this output as a useful starting point for several applications relating to the anthropogenic noise levels themselves. The models provide a quantitative framework for simulating the acoustic consequences of proposed industrial developments in BC, such as expansion of shipping ports and associated traffic near Prince Rupert, Kitimat and Vancouver. The models allow quantitative forecasting and hindcasting to assess how trends in shipping may translate to trends in noise levels. Most importantly, the predictions can be overlaid on marine wildlife distribution maps to evaluate impacts of anthropogenic noise on the critical habitats of vulnerable species.

Table of Contents

1. INTRODUCTION

Sound travels particularly well in the ocean, and aquatic species have evolved many adaptations to use sound for communication, navigation, foraging and predator avoidance. In the ocean, light attenuates so rapidly that vision is of practical use only on the scale of tens of meters, whereas some sounds may propagate over hundreds or thousands of kilometers. The ocean is naturally a noisy place, with ambient soundscapes featuring abiotic sounds (e.g., from wind, waves, subsea earthquakes and cracking ice) and biotic sounds (e.g., from fish, snapping shrimp and whales). In the deep ocean, low-frequency energy, such as that produced by baleen whale calls, is absorbed less and therefore propagates farther than high-frequency energy, such as dolphin whistles (Richardson *et al.*, 1995). These acoustic properties set the scene for remarkable innovation in the methods of sound production and reception used by a variety of marine taxa over evolutionary time scales. Among vertebrates, a wealth of information is available on sound production and reception in bony fish, elasmobranchs and marine mammals (Tyack and Clark, 2000). Some invertebrates, including crustaceans, produce and use sound to orient (Simpson *et al.*, 2011; Vermeij *et al.*, 2010), and the extent to which cephalopods and squid use sound is an area of active research (Mooney *et al.*, 2010). It is easy to imagine strong selection pressure acting on a variety of acoustic traits. The relationship between echolocating predators and their acoustically sensitive prey (e.g., dolphins and herring, or killer whales and seals) has been likened to an acoustic "arms race" that selects for specialised auditory systems (Tyack and Clark, 2000; Wilson and Dill, 2002). The vocal dialects of resident, fish-eating killer whale matrilines provide one of the strongest lines of evidence for culture in cetaceans (Deecke *et al.*, 2000). Put simply, sound is an essential element of the habitats of many marine organisms.

In the last century, human activities in the ocean have introduced a growing number of novel sound sources. Some of these tools exploit the same acoustic properties of the ocean that animals do, like the use of sonar to navigate or find fish, or seismic (airgun) arrays to find oil deposits under the seabed. Others, such as shipping or pile-driving, introduce acoustic energy unintentionally. The sheer scale of maritime shipping means that the 20-200 Hz frequency band in the ocean is now dominated by the sound of distant ships, throughout much of the northern hemisphere (Tyack, 2008). The peak energy of pile driving falls into the same frequency band (Erbe, 2009), and contributes significantly to the background din in Europe due to windfarm installations.

Anthropogenic underwater noise can have a multitude of potential impacts on marine life, ranging from mere audibility to behavioural reactions, communication masking, hearing impairment, stress and ultimately population-level impacts (Erbe, 2012). Much of the research on biological impacts of ocean noise has focused on short-term behavioural responses. In marine mammals, these studies have demonstrated that some acoustic stimuli can affect the behaviour of individuals, and that in certain circumstances involving extremely sensitive species, these can have lethal consequences (D'Amico *et al.*, 2009; Tyack, 2008).

Behavioural responses can take place over large spatial scales. Harbour porpoise can be displaced by the noise of pile-driving at a range exceeding 20 km (Tougaard *et al.*, 2009).

Beluga whales respond to icebreakers at up to 60 km in range (Cosens and Dueck, 1988; Cosens and Dueck, 1993; Erbe and Farmer, 2000b; Finley *et al.*, 1990). The biological cost of short-term avoidance responses is context-specific, but bioenergetics provides one link between short-term behavioural responses to fitness-level consequences that may lead to population-level effects. For example, food limitation is a factor in the at-risk status of north-eastern Pacific populations of fish-eating killer whales, which respond to repeated disturbance by reducing their time spent feeding (Williams *et al.*, 2006).

Ship noise reduces the communication space of baleen whales (Clark *et al.*, 2009). Even though most of the acoustic energy from ships is emitted at the low frequencies used by baleen whales, the ship spectrum at high frequencies can interfere with high-frequency cetacean communication. For example, in controlled behavioural studies, ship noise was shown to have a stronger potential for masking of beluga whale calls than naturally-occurring ice-cracking noise of similar broadband level (Erbe, 2000, 2008; Erbe and Farmer, 1998, 2000a; Erbe *et al.*, 1999).

Shipping noise could further disrupt signals used for orientation of larval stages of fish and invertebrates on coral reefs during their settlement phase, which could reduce recruitment or increase predation risk (Simpson *et al.*, 2005). Chronic exposure to shipping noise can cause physiological stress in large whales that could impact individual health and fitness (Rolland *et al.*, 2012). Anthropogenic noise has been shown to distract the vigilance behaviour or individual sticklebacks, and this act of shifting attention from foraging or predator evasion to respond to anthropogenic stimuli can carry fitness-level consequences (Purser and Radford, 2011).

In the last few years, there has been a paradigm shift in the way that researchers tackle the spatial and temporal scales of ocean noise. Ocean noise from shipping and other ubiquitous human activities is now being recognised as a chronic, large-scale, habitat-level stressor (Ellison *et al.*, 2011). This shifting emphasis has important implications for the way that ocean noise is managed and mitigated. When we think of noise as causing impacts at the level of the individual, typical management tools regulate activities within a certain distance of the animal in question (e.g., marine mammal observers monitoring an acoustic "safety zone" around seismic surveys, sonar exercises or pile-driving; or whale-watching guidelines that require boaters to maintain a certain distance from cetaceans). In contrast, when we consider noise as a habitat-level stressor, we invoke place-based management tools. This is reflected in recent moves toward assessing the total energy budget of human noise in waters under U.S. jurisdiction, and in the inclusion of anthropogenic noise in the European Union's Habitats Directive (Hatch and Fristrup, 2009). In Canada, the legal definition of critical habitat for resident killer whales acknowledges that "it is important that the threat of a degraded underwater acoustic environment be managed in critical habitat, in order that killer whales can maintain communication, and detect and capture prey while in the area" (Fisheries and Oceans Canada, 2011). What remains to be seen is how to scale up the available science on underwater noise to meet management needs on appropriate spatial and temporal scales.

While the concept of noise as a habitat-level stressor represents a recent development in the field of bioacoustics, the wider fields of systematic conservation planning and marine spatial planning have been working on these scales for decades. We see value in providing acoustic modelling tools to allow ocean noise to be accurately represented in marine spatial planning processes. Marine spatial planning provides a mechanism for implementing ecosystem-based management, and while the emphasis was originally focused on the design and management of marine protected areas (MPA), more recent zoning tools facilitate spatial solutions that allow multiple uses of marine space. In fact, the process of identifying conflicting objectives and proposing trade-offs to achieve multiple objectives is at the core of marine spatial planning. MPAs and marine zoning provide powerful ways to separate valued and vulnerable biodiversity elements from anthropogenic stressors, so the process of mitigating impacts of ocean noise on marine wildlife would seem to be ideally suited to a marine spatial planning framework. A number of efforts are underway to compile information on human activities in the world's oceans, to identify areas where anthropogenic activities most strongly overlap with vulnerable marine ecosystems (Halpern *et al.*, 2008). To date, such conservation assessments have included an impressive suite of anthropogenic stressors, but have not yet considered ocean noise. In our view, this oversight stems from a general lack of analytical tools to provide reasonable predictions of the human-generated contribution to ocean noise in the vast stretches of ocean that have not been sampled acoustically. The algorithms used in most decision-support software tend to gravitate toward data-rich areas (Moilanen *et al.*, 2009). This has important implications for managing noise in the ocean, because acoustic measurements are made at relatively few points, whereas tools to support spatial planning benefit from having data in the form of surfaces. In order to bridge this gap, we developed models to predict the contribution of shipping activity to ambient ocean noise levels throughout BC waters, by integrating noise energy over time and space to produce a map of cumulative sound exposure levels throughout our study region. Our main objective was to produce a map of total acoustic energy of underwater ship noise received over a full year (2008) off western Canada.

2. METHODS

2.1. SHIPPING DATA

2.1.1. TRAFFIC HOURS

Ship noise levels were predicted from a geo-referenced database on ship traffic provided by the Vessel Traffic Operation Support System (VTOSS) program of MCTS (Marine Communications and Traffic Services of the Canadian Coast Guard/Fisheries and Oceans Canada). The MCTS database compiles information on vessel type, ship location and speed in a 5 km gridded format that has been described previously (Hilliard and Pelot, 2011). Data on ship traffic for 2008 provide minimum estimates of ship densities travelling through the Canadian Exclusive Economic Zone (EEZ), because small vessels and those bound for non-Canadian ports are not required to identify themselves to MCTS. Ship positions in the MCTS database are derived from radio call-ins, radar tracking and interpolation of positions at four-minute intervals for all ships tracked. The MCTS database was used to compile a table that included counts, speed (and standard deviation) of all vessel types using the Canadian Pacific EEZ in 2008. Given the constraints of the shipping database, ship counts could be summarized either by ship length or vessel type (Table X and Y). For the purposes of choosing appropriate acoustic source levels, we used the length table, because of better correlation of source level with length rather than type. The MCTS database was used to estimate total cumulative hours for all ship length categories within all 5 km x 5 km grid cells for the entire EEZ.

Table 1: Vessel classes by length

L1	Length ≤ 10 m
L2	10 m < Length ≤ 25 m
L3	25 m < Length ≤ 50 m
L4	50 m < Length ≤ 100 m
L5	100 m < Length ≤ 200 m
L6	200 m < Length ≤ 290 m
L7	Length > 290 m

Table 2: Vessel classes by type

T1	Passenger / cruise vessels
T2	Fishing vessels
T3	Government vessels
T4	Pleasure vessels and yachts
T5	Merchant (bulk / cargo) vessels
T6	Tanker vessels
T7	Research vessels

We used the length classes (Table 1), because of higher correlation of source level with length rather than type.

Figure 1 shows the cumulative number of hours that vessels of all classes spent in each grid cell of 5 km x 5 km size over the year of 2008. The year 2008 had 8784 hours. The

maximum number of traffic hours recorded is greater than this. The maximum number of traffic hours was 27,522, which is three times as many hours as there were in the year 2008. The reason for this is that traffic hours were added over all vessels. If two vessels traversed a grid cell at the same time, sailing side-by-side, and each took 30 minutes, then this was counted as one full hour of traffic. This was necessary in order to compute the total acoustic energy from all ships, and energy is additive. In other words, the cell with the maximum number of traffic hours recorded had on average three vessels per hour for the entire year (day and night). This cell was near the port of Seattle.

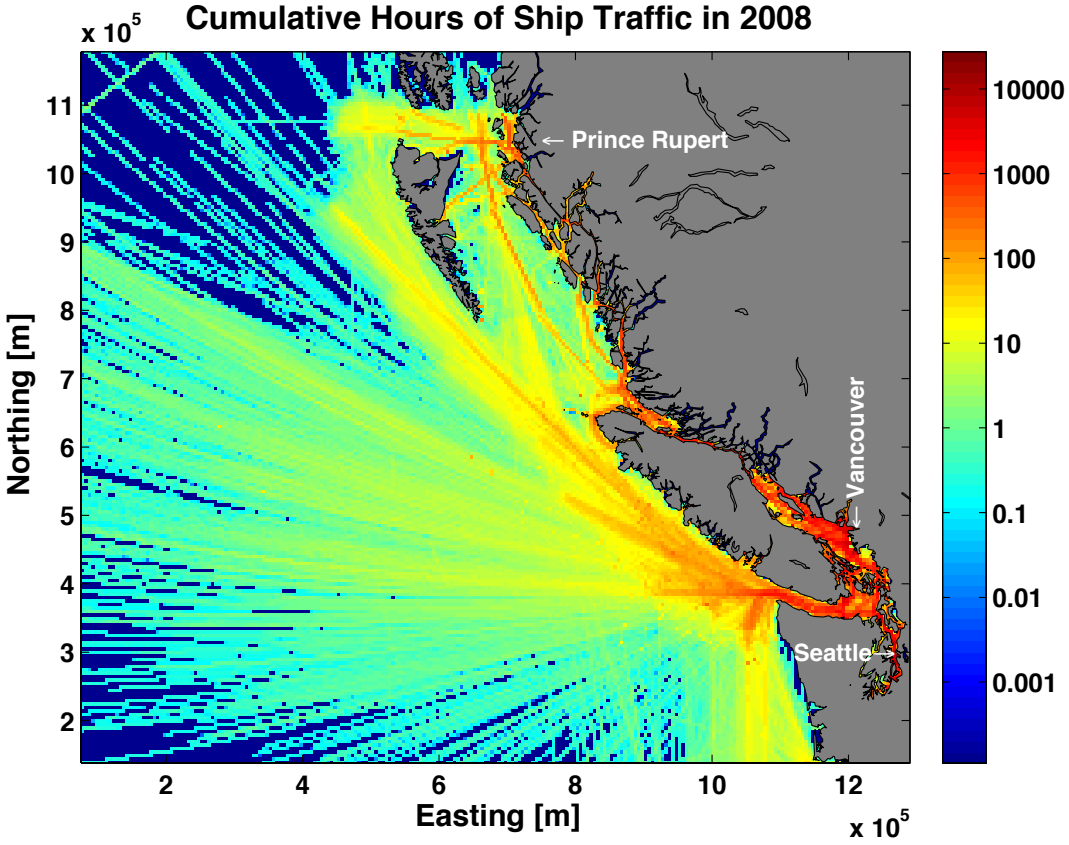

Figure 1: Total hours of shipping for the year 2008.

2.1.2. Source Spectra

Underwater noise from vessels originates predominantly from propeller cavitation and hull-borne machine vibration (Ross, 1976). While every vessel has a unique acoustic signature, it is possible to derive representative source spectra for different classes of vessels that are suitable for modelling ship noise over broad spatial and temporal scales (National Research Council, 2003). For this study, we used the shipping source spectral density formulae from the Research Ambient Noise Directionality model RANDI 3.1 (Breeding *et al.*, 1994; Wagstaff, 1973). RANDI estimates source spectral density levels (dB re 1 µPa/√Hz @ 1 m) from ship length and ship speed, according to Ross's classic power-law model:

$$L_s(f,v,l) = L_{s0}(f) + c_V \times 10\log_{10}(v/v_0) + c_L \times 10\log_{10}(l/l_0) + g(f,l)$$

In this formula, c_V and c_L are power-law coefficients for speed and length (taken to be 6 and 2, respectively), v_0 is the reference speed (12 kt), l_0 is the reference length (300 ft),

$L_{s0}(f)$ is a mean reference spectrum, and $g(f,l)$ is an additional length-dependent correction to the Ross model (Breeding *et al.*, 1996).

For this work, representative 1/3-octave band source spectra were modelled for each of the seven vessel-length categories (L1-L7) present in the shipping traffic database (Figure 2). Speed and length statistics from the database were used to derive a representative speed and length for each category (Table 3). Greater weight was assigned to the fastest vessels in each category, according to the assumed sixth-power dependence of radiated sound power on ship speed. Similarly, greater weight was assigned to larger vessels in each category, according to the second-power dependence of radiated sound power on ship length. As a result, the 1/3-octave band source spectra represent the mean source level, in terms of total radiated sound power, for each category of vessel.

Table 3: Modelled properties for the seven vessel length classes in the shipping traffic database. Representative length, speed, and source depth for each category were derived according to the procedures described in the text.

Vessel Class	**L1**	**L2**	**L3**	**L4**	**L5–L7**
Lengths represented (m)	≤ 10	10-25	25-50	50-100	≥ 100
Modelled length (m)	7.8	18.6	38.9	77.8	155.6
Modelled speed (kts)	15.6	9.1	14.6	13.6	15.0
Modelled source depth (m)	0.5	1.25	3.0	6.0	6.0
Broadband SL (dB re 1 µPa @ 1 m)	163.6	157.2	176.4	181.1	190.8

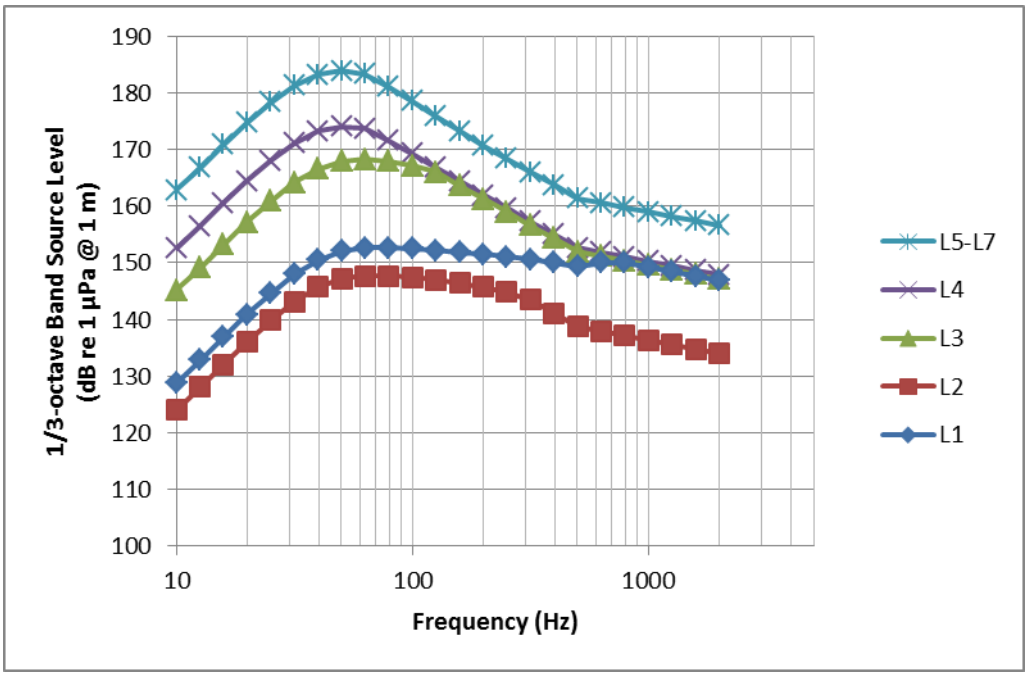

Figure 2: Mean 1/3-octave band source levels for the seven vessel length classes in the shipping traffic database, computed according to the parameters listed in Table 3.

Published measurements for merchant ships indicate that, for vessels longer than about 150 m, source level is largely independent of length and speed (Scrimger and Heitmeyer, 1991; Wales and Heitmeyer, 2002). Furthermore, comparisons of the RANDI estimates with measurements of large merchant vessels from McKenna *et al.* (2012) indicate that

RANDI significantly overestimates source levels for 200-300 m ships. Therefore, the source levels of the L6 and L7 classes (vessels ≥ 200 m length) were taken to be identical to the L5 class (100-200 m length) so as not to overestimate the contribution of very large ships to the cumulative noise budget.

The shape of the reference source spectrum in RANDI is largely independent of vessel length, and therefore does a poor job of accurately representing the spectral features of small boats (classes L1 and L2). Published source level measurements for small boats, such as whale-watching boats and fishing boats, indicate that their dominant sound emissions are at higher frequencies than larger vessels (Erbe, 2002; Richardson *et al.*, 1995; Williams *et al.*, 2002a). This is due to their smaller, shallower propellers which have higher blade rates, and increased surface-dipole cancellation at low frequencies. To the best of the authors' knowledge, however, there have been no comprehensive studies of mean source characteristics for small boats to date.

The effect of source depth on radiated sound power was taken into account by applying a frequency-dependent correction to the source spectra for each vessel category. Source depths for each category were taken to be proportional to vessel length, up to a maximum depth of 6 m, which is a typical mean source depth for merchant shipping (Scrimger and Heitmeyer, 1991). To account for the effect of surface-dipole interference on radiated sound power, source levels at wavelengths greater than four times the source depth were attenuated according to the relation given by Brekhovskikh and Lysanov (2003)(Eq. 4.1.24). The attenuation was applied to the spectra on a relative basis only: the broadband source level for each category was preserved, so as not to underestimate source levels for the smallest vessels. After the source depth correction was applied, the spectra for the smallest vessels (L1 and L2) were much flatter and better represented measurements of sound emissions from small vessels (Erbe, 2002).

2.2. Environmental Parameters

2.2.1. Bathymetry

Bathymetry was extrapolated from the Etopo2 database[1] with 2-minute resolution to the 5 km x 5 km grid of the shipping database. The British Columbia coastline was extracted from the Global Self-consistent, Hierarchical, High-resolution Shoreline Database (GSHHS)[2]. Figure 3 shows the bathymetry of the modelling area.

[1] http://www.ngdc.noaa.gov/mgg/global/etopo2.html
[2] http://www.ngdc.noaa.gov/mgg/shorelines/gshhs.html

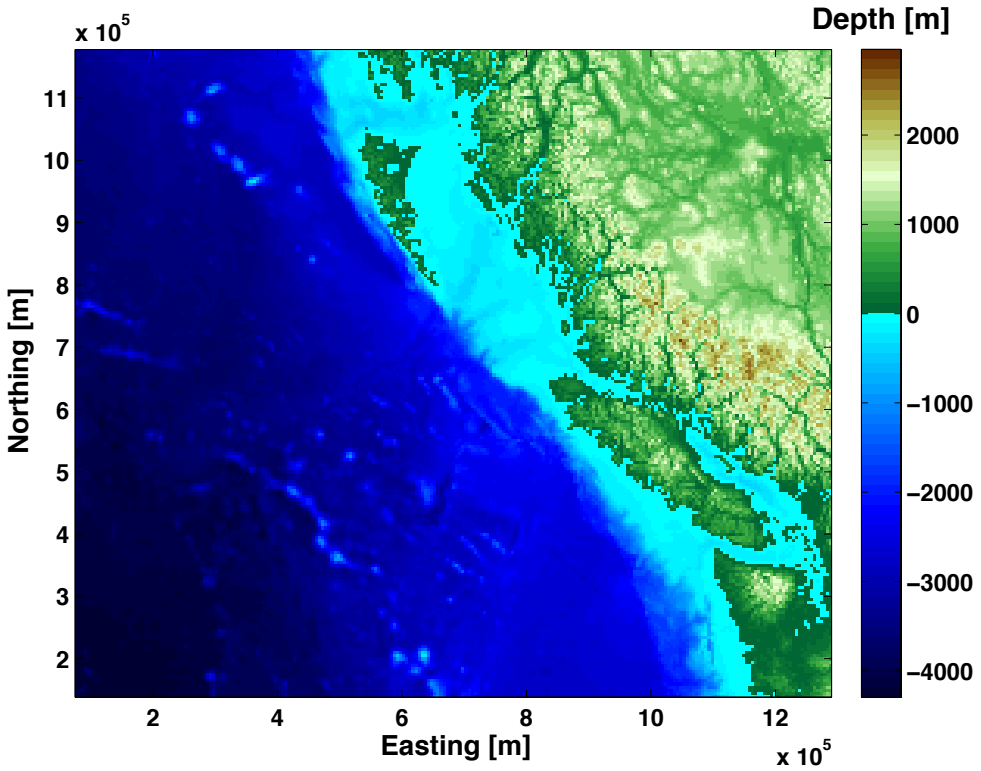

Figure 3: Bathymetry of modelled area.

2.2.2. GEOACOUSTICS

The geoacoustic properties of the seabed strongly influence acoustic transmission loss over the continental margins. This is because reflection and absorption of sound energy at the seabed is a dominant loss mechanism in shallow water (Urick, 1983). Direct measurements of the geoacoustic properties of the seabed are seldom available. Most often, these must be inferred from a physical description of the materials compositing the seabed, such as sediment porosity or rock type (Hamilton, 1980). Lack of reliable measurements of the geoacoustic properties of the seabed is a major source of uncertainty when modelling acoustic transmission loss for continental shelf locations.

For this work, our goal was to perform a sensitivity analysis to quantify the influence of geoacoustic uncertainty on transmission loss. To this end, a range of geoacoustic models were derived based on available seabed classification data for different areas of BC marine waters. Seabed geoacoustics were based primarily on a large database of surface and sub-surface sediment grain-size samples, provided by the Geological Survey of Canada (GSC) (Figure 4). Where the GSC data lacked coverage, seabed type was estimated from the BC Marine Ecological Classification (BCMEC) maps published by the Ministry of Sustainable Resource Management (Howes *et al.*, 1997)

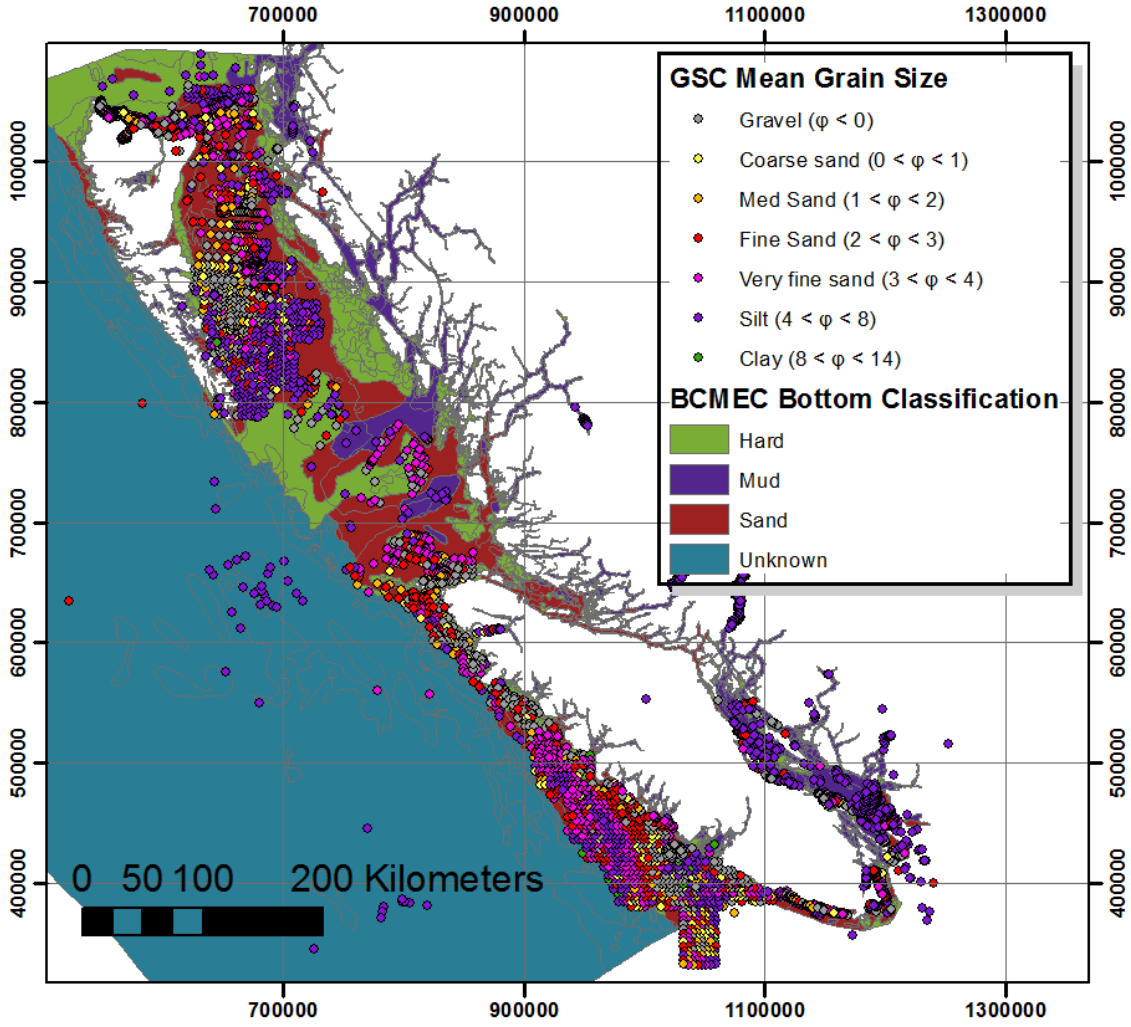

Figure 4: Map of GSC mean sediment grain size samples and BCMEC bottom type classification. Grid units are BC Albers (NAD83) Easting and Northing (m).

Geoacoustic profiles were derived for the ten different sound-propagation transects used in the error analysis (see Section 2.4). The bottom type along each transect was classified as either sandy or silty—or a range-dependent combination of the two—based on the mean grain size samples from the GSC database (Table 4). The effect of geoacoustic uncertainty on transmission loss was investigated by modelling two different kinds of seabed types for each transect, one acoustically hard (i.e., more-reflective) and the other acoustically soft (i.e., less-reflective). To simulate these conditions, the geoacoustic properties of the seabed were varied according to limiting grain size values: $\varphi = 5$ (sandy silt) and $\varphi = 7$ (clayey silt) for silt areas, and $\varphi = 0.5$ (coarse sand) and $\varphi = 2.5$ (fine sand) for sand areas. The geological grain size parameter φ is equal to $-\log_2$(grain diameter/mm). The grain-shearing model of Buckingham (2005) was used to compute geoacoustic properties of the sediments (P-wave speed, S-wave speed, density, P-wave attenuation, and S-wave attenuation) from grain size (example shown in Table 5).

Table 4: Modelled seabed sediment composition and thickness along each of the ten PE model transects. Transects TL1, TL7, and TL10 were modelled using a range-dependent combination of both seabed types. Sediment thickness corresponds to the depth of the acoustic basement (sedimentary rock) below the seabed.

Transect	Silt Seabed (ϕ = 5-7)	Sand Seabed (ϕ = 0.5-2.5)	Layer Thickness (m)
TL1	X	X	10-20
TL2	X		20-40
TL3	X		20-40
TL4	X		20-40
TL5		X	10-20
TL6		X	10-20
TL7	X	X	10-20
TL8	X		10-20
TL9	X†		—
TL10	X	X	10-20

† For transect TL9, abyssal plain sediments were taken to have mean grain size ϕ = 7.5, following Hamilton (1980).

Table 5: Geoacoustic model parameters for soft silt (phi = 7) bottom type. Geoacoustic properties for silt were derived using Buckingham's Grain-Shearing model. S-wave properties of the marine sediments were modelled only for the top-most layer. MBSF = metres below seafloor.

Material	MBSF	Grain Size (ϕ)	Density (/water)	P-wave Speed (m/s)	P-wave Attn. (dB/λ)	S-wave Speed (m/s)	S-wave Attn. (dB/λ)
Clayey Silt	0.5	7	1.620	1461.8	0.156	98	0.108
	2.5	7	1.620	1484.9	0.264	-	-
	5	7	1.620	1499.6	0.331	-	-
	10	7	1.620	1518.5	0.413	-	-
	20	7	1.620	1542.7	0.514	-	-
Sedimentary	20	-	2.189	2200.0	0.100	-	-
Rock	115	-	2.189	2298.4	0.100	-	-
	215	-	2.189	2421.4	0.100	-	-

For continental shelf areas, the effect of surficial sediment thickness on transmission loss was also considered by varying the depth to the acoustic basement in the geoacoustic model. There is very little published information on seabed sediment thickness for the BC offshore; however, available data suggest that sediment layering is non-uniform in many places and the thickness is variable. For the error analysis, a typical range of sediment thickness was selected based on interpreted Huntec cross sections and core data from published studies (Barrie and Bornhold, 1989; Barrie and Hill, 2004; Barrie *et al.*, 1990; Bornhold and Barrie, 1991). Sediments were assumed to be thicker in the Salish Sea, due to alluvial deposition from the Fraser River outflow. The acoustic basement below the sediments was assumed to consist of lithified tertiary sediments, with associated geoacoustic properties (MacGillivray, 2006). Thicker and thinner sediments were associated with the acoustically soft and hard seabed models, respectively.

2.2.3. HYDROACOUSTICS

The sound speed profile in the ocean strongly influences long-range acoustic propagation by refracting and trapping sound energy in the water column. The speed of sound in seawater is a function of temperature, salinity and depth. Because temperature and salinity are horizontally stratified in the ocean, vertical features of the sound speed profile are stable over large distance scales (typically tens to hundreds of kilometres). Temperature and salinity are not static in time, however, and changes occur on diurnal and seasonal time scales due to oceanographic mixing and transport processes.

Seasonal changes in the shape of the sound speed profile can have a large effect on transmission loss in the ocean. In order to quantify the influence of sound speed profile variability on transmission loss, we considered both February and August water column conditions in the error analysis. For each transect, range-dependent profiles of mean ocean temperature and salinity were interpolated from the GDEM (Global Digital Environmental Model) database (Carnes, 2009) at 10 km spacing. Speed of sound in seawater was computed from temperature, salinity, and depth using the formulae of Clay and Medwin (1977). For the BC offshore, seasonal sound speed profiles exhibit the greatest variability in the upper 200 m of the water column (Figure 5). Summer insolation in August results in a strongly downward-refracting profile. Wind-driven mixing combined with atmospheric cooling in February results in a mild surface-duct profile.

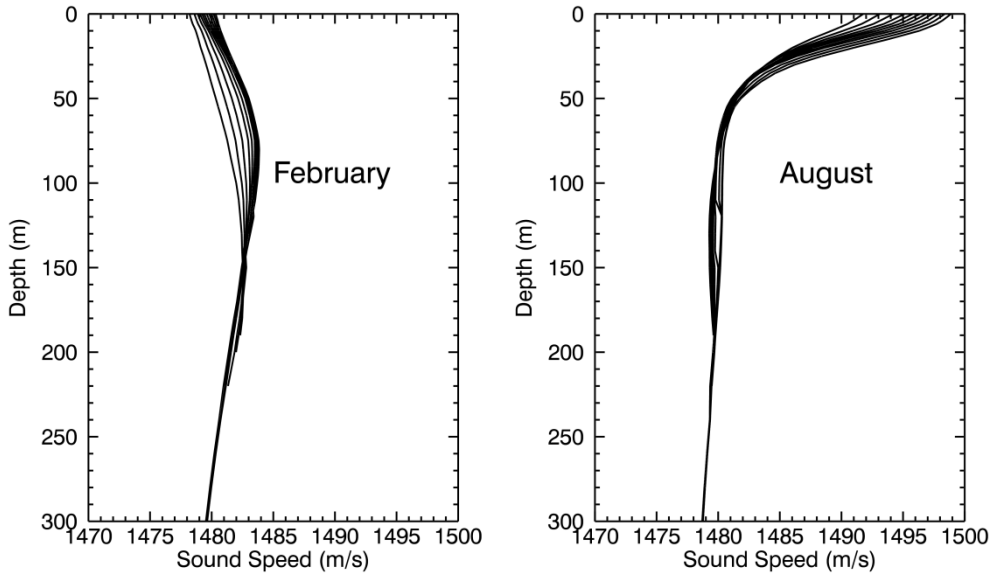

Figure 5: GDEM sound speed profiles along the first 100 km of transect TL1 for February and August conditions. Profiles are sampled every 10 km range via bilinear interpolation of the GDEM grid.

2.3. CUMULATIVE MODEL

2.3.1. DETERMINING SOURCE-RECEIVER PAIRS

As a first step, the model connected all 5 km x 5 km grid cells that included water with each other yielding all possible source-receiver transects. Any of these straight-line

transects that crossed land were discarded. The lengths of all remaining transects were computed. All cell pairs that were less than 100 km apart qualified as source-receiver pairs for further modelling.

2.3.2. TRANSMISSION LOSS

Transmission loss was computed for all water-borne transects shorter than 100 km. Beyond 100 km, acoustic energy had dissipated to a degree where it no longer contributed significantly to the cumulative noise map; the transmission loss was modelled in excess of 80 dB over all transects and for all frequencies and hydro- and geo-acoustic profiles (see Figure 9).

A geometric spreading model was applied accounting for spherical spreading to the maximum water depth D_{max} along the transect and cylindrical spreading for the remainder of the transect. Frequency-dependent, volumetric absorption TL_a was also computed. For ranges $R > D_{max}$ (both in units of metres), the transmission loss TL becomes:

$$TL = 20\log_{10} D_{\max} + 10\log_{10}\frac{R}{D_{\max}} + TL_a$$

For ranges $R < D_{max}$, the transmission loss simply becomes:

$$TL = 20\log_{10} R + TL_a$$

The frequency-dependent absorption loss TL_a was computed according to:

$$TL_a = \alpha R / 1000$$

where the absorption coefficient α is (François and Garrison, 1982a, 1982b):

$$\alpha = 0.106\frac{f_1 f^2}{f_1^2 + f^2}e^{(pH-8)/0.56} + 0.52\left(1+\frac{T}{43}\right)\frac{S}{35}\frac{f_2 f^2}{f_2^2 + f^2}e^{-z/6} + 4.9\times10^{-4} f^2 e^{-(T/27+z/17)}$$

with $f_1 = 0.78(S/35)^{1/2}e^{T/26}$ and $f_2 = 42e^{T/17}$; f in kHz, and α in dB/km.

This equation is valid for the following ranges in temperature T, salinity S, depth z and pH:

$-6 < T < 35$°C (S=35ppt, pH=8, z=0)

$7.7 < pH < 8.3$ (T=10°C, S=35ppt, z=0)

$5 < S < 50$ppt (T=10°C, pH=8, z=0)

$0 < z < 7$km (T=10°C, S=35ppt, pH=8)

Transmission loss was computed for the centre frequencies of adjacent 1/3 octave bands from 10 Hz to 2 kHz. Considering the ocean an acoustic waveguide, in the case of a

hard (reflective) seafloor, the minimum frequency that can propagate has a wavelength λ of four times the minimum water depth D_{min}:

$$\lambda_{\max} / 4 = D_{\min}$$

For each source-receiver pair, D_{min} was found and a cut-off frequency imposed, below which no energy was allowed to propagate.

2.3.3. Received Levels

The 1/3 octave band source spectra (in dB) were added to the transmission loss (in dB) for all source-receiver pairs and all frequencies. To convert from root-mean-square sound pressure level (SPLrms) to sound exposure level (SEL), a term reflecting the number of hours *H* a vessel class spent in each source cell was added:

$$SEL = SPL_{rms} + 10\log_{10} H$$

The received level in a source cell was computed as the source level plus the transmission loss for an average distance to the cell centre of 1.9 km in a 5 km x 5 km cell, plus the contribution from sources outside of this cell.

2.3.4. Cumulative Noise Map

Finally, sound exposures in each receiver cell were summed over all vessel classes in linear (not logarithmic) terms. Converting the summed exposures back to dB resulted in a map of cumulative sound exposure level over all vessel classes.

2.4. Error Analysis

We performed a sensitivity analysis of the transmission loss model to variability of environmental parameters by comparison to a range-dependent parabolic equation (PE) model along ten selected transects (Figure 6). PE models compute transmission loss by solving an approximate one-way wave equation that neglects back-scattered sound energy. They are the most efficient class of acoustic model for computing sound propagation at low frequencies in range-dependent environments. For this study, we employed a variant of the RAM propagation model (Collins *et al.*, 1996), which has been modified to account for shear wave conversion at the seabed using the complex-density equivalent fluid bottom approximation of Zhang and Tindle (1995). RAM solves range-dependent ocean acoustics problems, with arbitrary bottom layering, and correctly accounts for steep propagation angles by using a wide-angle, Pade series expansion of the PE operator.

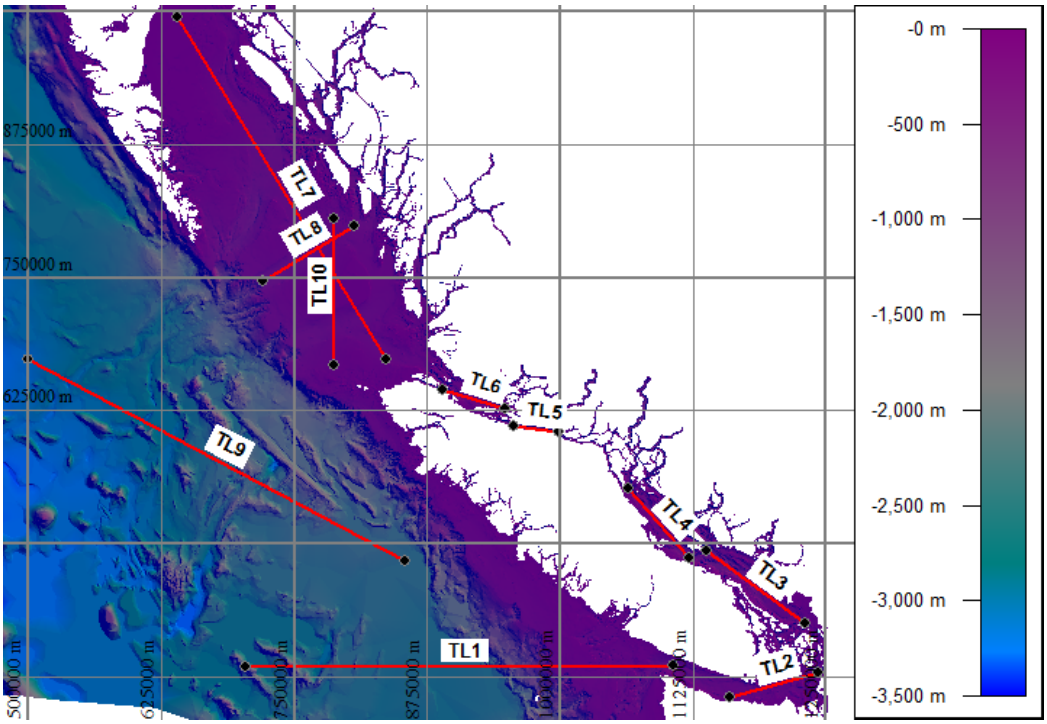

Figure 6: Map showing the ten PE model transects (TL1-TL10) used for the transmission loss error analysis. Bathymetry data are from the high-resolution Living Ocean Society (LOS) database. The bathymetry scale is shown on the right. Grid units are BC Albers (NAD83) Easting and Northing (metres).

Baird *et al.* (2005) tagged 34 killer whales in southern British Columbia with time-depth recorders to measure dive profiles. While these animals spent most of their time in the top 5 m of water, they occasionally dove all the way to the seafloor. The maximum depth recorded was 264 m. Animals dove to > 150 m only once every 5 h. We therefore averaged the modelled transmission loss over the top 150 m of water.

Along each PE transect, transmission loss was computed every 500 m in range and every 10 m in depth down to 150 m. A source depth of 6 m was assumed for the PE model. Transmission loss versus range was modelled at 24 1/3-octave band centre frequencies from 10 Hz to 2000 Hz. Bathymetry profiles for the ten transects were obtained from a high-resolution (100 m) digital bathymetry map for the BC offshore compiled by the Living Ocean Society (LOS). Along each model transect, water depth was extracted every 50 m in range via bilinear interpolation of the gridded bathymetry data. Two different bottom types (hard and soft extremes of the prevalent geology) and two different sound speed profiles (February and August representing the winter and summer extremes) were modelled for each transect (see Sections 2.2.2 and 2.2.3). Curves of transmission loss versus range from the PE model were corrected to include the contribution of seawater absorption, according to the formulae of Francois and Garrison (1982 a,b).

The resulting ensemble of PE model predictions, for the ten selected transects, was used to quantify the sensitivity of the acoustic transmission loss estimates to seafloor type, water parameters and bathymetry (Section 4.2). Uncertainty was further assessed by comparison to measured transmission loss in northern BC (Austin *et al.*, 2010).

3. RESULTS

The resulting map of cumulative underwater acoustic energy from all ships over a 12-month duration in the year 2008 is shown in Figure 7. Plotted are sound exposure levels (SEL) in dB re 1 µPa²s. All vessel classes were included. Noise levels were highest in the Straits of Georgia and Juan de Fuca near the ports of Vancouver and Seattle, then Prince Rupert. The maximum modelled sound exposure level was 215 dB re 1 µPa²s near Seattle.

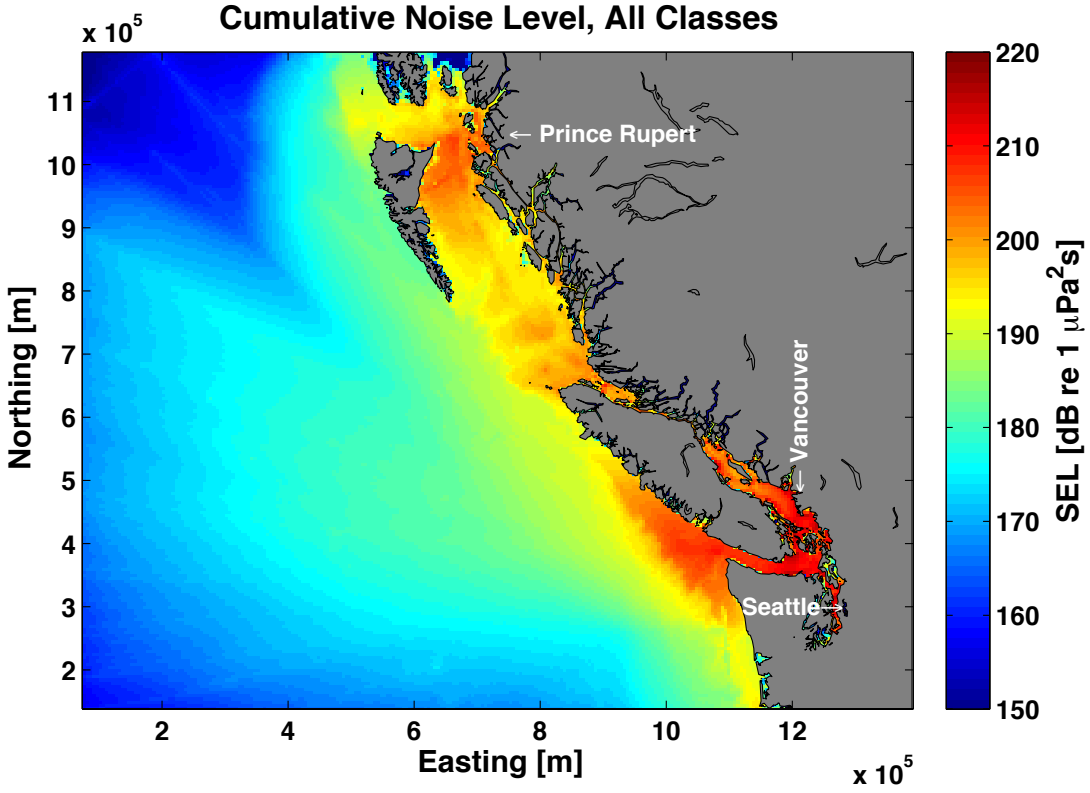

Figure 7: Cumulative sound exposure level from vessel traffic from Jan – Dec 2008.

4. DISCUSSION

The following sections present a sensitivity analysis of the cumulative noise model to variability in seafloor geology, water parameters (sound speed profiles) and bathymetry; as well as an error analysis of the source data and resulting map.

4.1. UNCERTAINTY OF THE TRAFFIC DATA

The VTOSS shipping database provides the best available snapshot of shipping traffic in western Canadian waters over an entire year, but it does have its limitations. Small vessels and private yachts are underrepresented in the database as they do not have to log their GPS positions. What percentage of large commercial vessels is missed (if any at all) is unknown. The database can be considered a minimum representation of ship traffic.

Positional data are necessarily coarse, because they represent straight-line interpolations between call-in sites. Speeds are imprecise for the same reason, although there is no reason to believe that they are biased in a systematic way. Privacy restrictions preclude identifying individual vessel identity, which is unfortunate, because reduction of ship noise overall would benefit from targeting the noisiest individual ships rather than requiring fleet-wide modifications. Finally, although Canada's economy suffered less during the 2008 downturn than other nations, it would be better to provide annual maps than to rely on any single year to provide a representative snapshot of shipping traffic for a region.

The noise map in Figure 7 tracks the vessel transects. Incomplete transect records can affect the noise map. Figure 8 shows an incomplete transect offshore Vancouver Island for vessel class 1, and several unfinished offshore transects for classes 4 and 7. Small vessels (classes 1 and 2) can be expected to stay inshore, however, broken offshore transects are also visible for these classes.

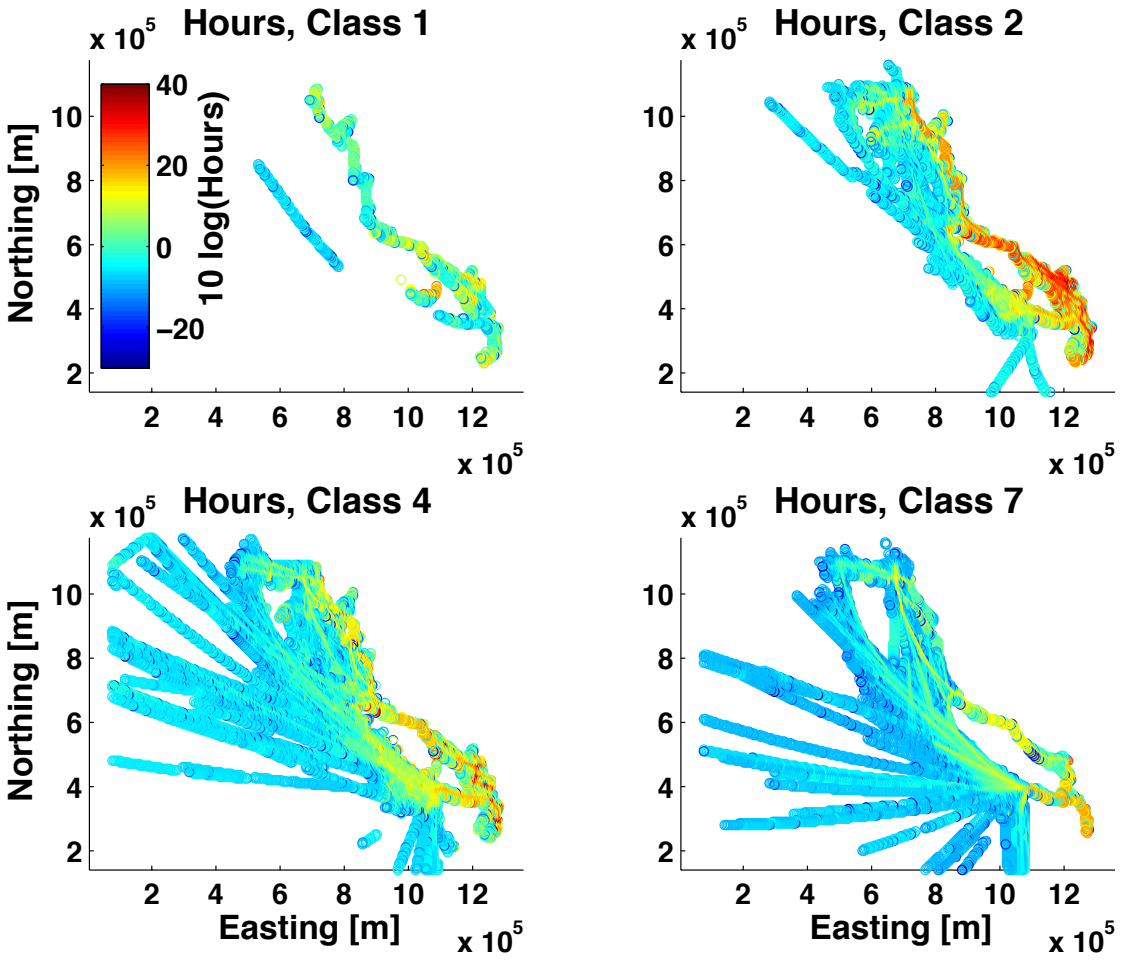

Figure 8: Traffic hours for four vessel classes showing 'broken' and 'incomplete' transects.

4.2. Uncertainty of the Ship Source Spectra

Scrimger and Heitmeyer (1991) collated source spectra of 50 merchant vessels. The range in spectral density levels was 30 dB, the standard deviation was 5.0 dB in the 70 – 200 Hz band, increasing to 6.8 dB in the 400 – 700 Hz band. This is the only publication of a statistical distribution of source spectra of that many ships within any one class. In the absence of similar studies for smaller vessel classes, we assume a standard deviation of < 7 dB of source spectra for all classes.

The source level of a ship depends on its speed and our source model can account for speed dependence. Dr. Patrick O'Hara of the University of Victoria kindly computed vessel speed by geographic area from the underlying shipping database. While we had expected to see speeds differ from offshore to inshore within each vessel class, this was not the case. Large vessels only slowed down very close to port at ranges not resolved by our 5 km x 5 km grid.

4.3. Uncertainty of the Transmission Loss Model

The PE modelling showed that transmission loss was frequency-dependent and influenced by the physical environment (*i.e.*, bathymetry, geoacoustics, and sound speed profile).

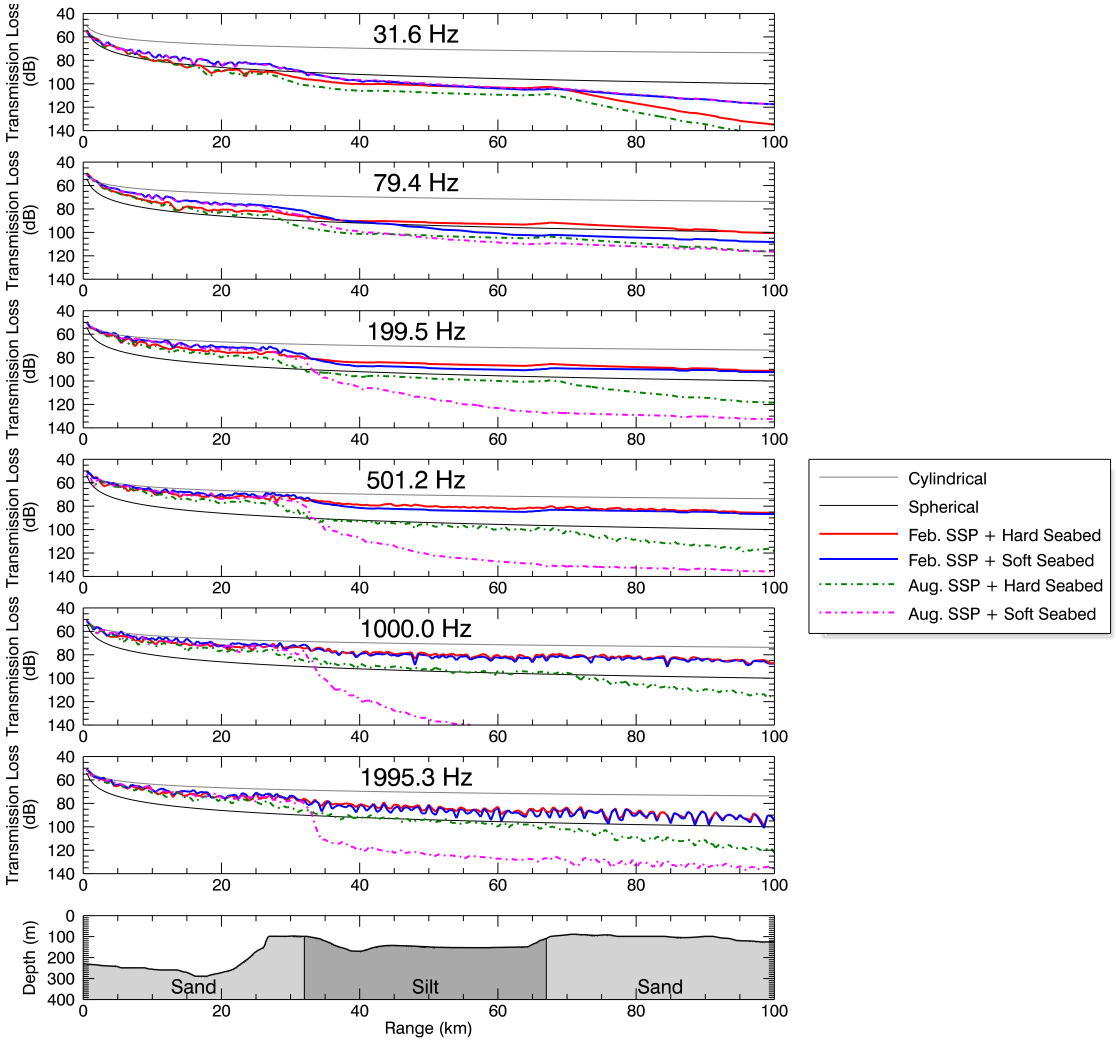

Figure 9: Transmission loss versus range along the first 100 km of transect TL1, as computed by the PE model at six frequencies (top six plots). The four coloured lines in each plot correspond to the four different sets of environmental parameters considered in the sensitivity analysis (SSP = sound speed profile). Transmission loss was averaged over the upper 150 m of the water column (up to the maximum water depth). The dark grey line shows the spherical spreading law, the light grey line changes from spherical to cylindrical spreading at 300 m range. Bottom plot shows bathymetry and seabed type along the model transect.

Figure 9 shows transmission loss modelled at several different frequencies along the first 100 km of transect TL1. Energy at low frequencies (plotted at 31.6 Hz) was lost according to spherical spreading to about 25 km in range. The bathymetry rose from 300 m at 20 km range to 100 m at 27 km range. Energy at low frequencies was "stripped", indicated by a drop in all four transmission loss curves (increase in transmission loss). Low-frequency energy dropped even more at 67 km range in the case of the 'harder' geoacoustic parameters (red and green lines).

Energy at higher frequencies followed a spherical spreading loss over the first few hundred meters, then changed to cylindrical spreading loss. In the cases of the summer sound speed profile (green and magenta lines), the environment was downward refracting, increasing the interaction of the sound with the seafloor. This is evident from a sudden increase in transmission loss at 25 km due to the rise in bathymetry (green line, hard seafloor) as well as at 33 km due to the change from sand to silt (magenta line, soft seafloor). The softer seafloor absorbed more sound than the harder (hence more reflective) seafloor.

The transmission loss curves for this transect clearly show how the effects of the environment are interrelated, how they depend on frequency, and how they accumulate with distance.

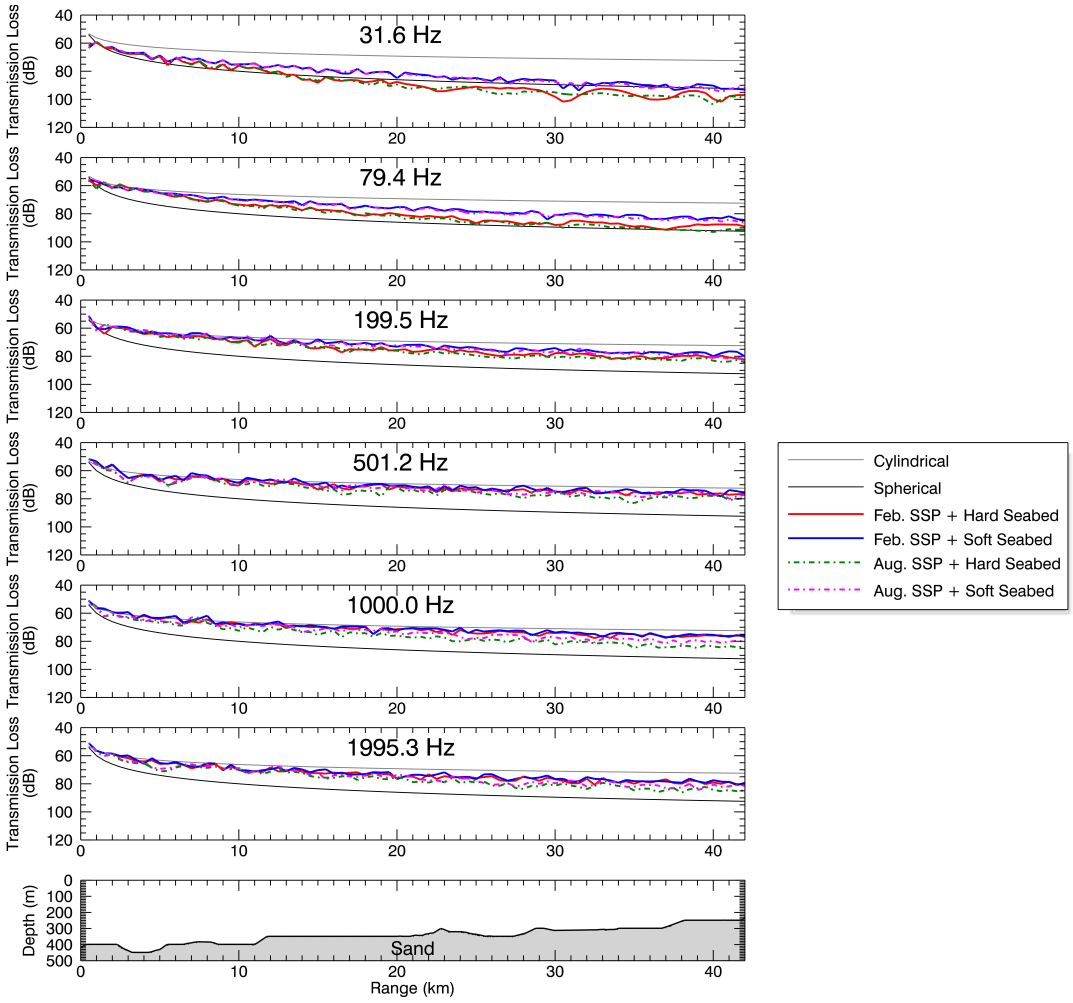

Figure 10: Transmission loss over transect TL5. Coloured lines represent the PE model; the dark grey line represents spherical spreading only; the light grey line represents a combination of spherical spreading (to 300 m range) and cylindrical spreading (at ranges > 300 m).

Along transect TL5 (Figure 10), the bathymetry was smoother than along TL1 (Figure 9), the seabed consisted of sand only. Transmission loss was greater at the low frequencies, and stayed within the bounds of spherical and cylindrical spreading for all

frequencies, the two extremes of the sound speed profile and the two limits of the seafloor parameters modelled.

To quantify the error of the transmission loss model due to the variability of bathymetry, geology and water parameters, the ensemble of transmission loss curves from the PE model (for TL1–TL10) was analysed statistically. For each frequency, transmission loss percentile levels (5%, 25%, 50%, 75%, and 95%) were computed from the distribution of PE model results at each receiver range, out to a maximum distance of 100 km. The resulting contours provided an estimate of the range-dependent probability density for transmission loss off the British Columbia coast (Figure 11).

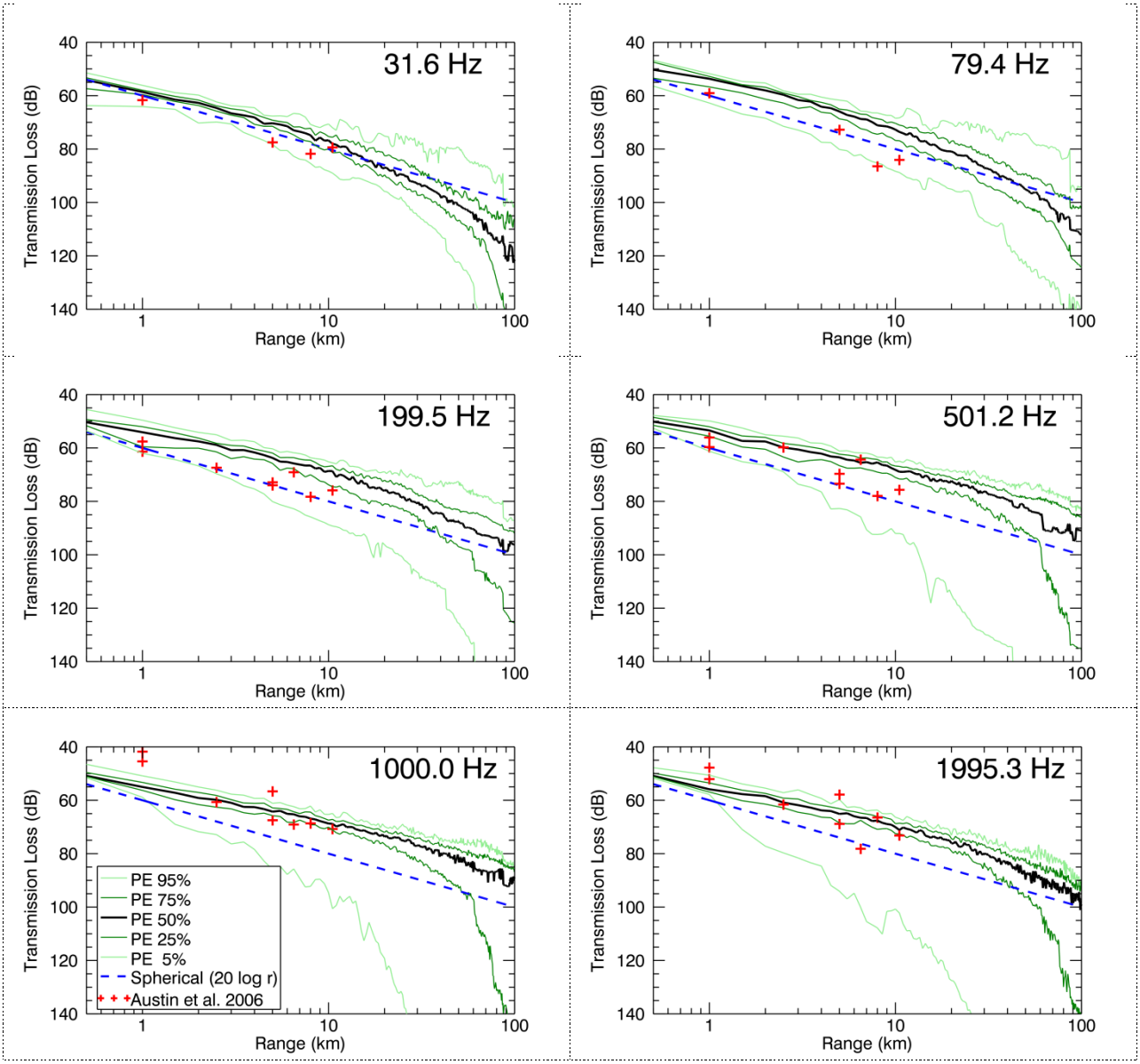

Figure 11: Transmission loss versus range statistics at six frequencies, as computed from the ensemble of PE model transects. Solid lines show the 5th, 25th, 50th, 75th, and 95th percentile transmission loss contours. Red crosses are transmission loss measurements from Austin et al. (2010) obtained off the north coast of BC. Blue dashed line indicates spherical spreading transmission loss.

The extremes of the transmission loss curves corresponded to the inshore transects. Offshore, in deep water, transmission loss followed a geometric model very closely thanks to a lack of environmental variability and a lack of seafloor interaction.

The statistical analysis showed that uncertainty in the transmission loss increased with range and that the uncertainty was generally greater at higher frequencies. At frequencies < 40 Hz, the median (*i.e.,* 50th percentile) transmission loss followed a spherical spreading law very closely (to within 3 dB) over ranges < 30 km. Median transmission loss was greater than spherical at longer ranges. At higher frequencies, the median transmission loss started out spherical and turned to cylindrical, as indicated by a median slope of 10 dB / decade in range, compared to 20 dB / decade in range for spherical spreading only. This conversion from spherical to cylindrical spreading was therefore included in the simple transmission loss model (see Section 2.3.2.).

The model results were also compared to field measurements of transmission loss (Austin *et al.*, 2010), in order to verify that they were representative of conditions in the BC offshore. These measurements were collected off the north coast of BC, in Caamano Sound and Principe Channel (situated at the eastern margin of Hecate Strait), in late September 2005. The measurements were collected using a controlled sound source, deployed at 4 m depth, and a bottom-mounted hydrophone recorder, deployed at 142 m and 214 m depth. Comparison with the percentile contours showed that most of the field measurements fell inside the 90% probability range of transmission loss values predicted by the PE model, except for a few outliers at 1 kHz and 2 kHz. The reason for these high-frequency outliers is unknown, but they may be due to the fact that the field measurements were obtained at a single depth: the depth-averaging employed in the PE model tends to smooth out extrema in the transmission loss curve. The high-frequency measurements could also have been affected by surface and seabed roughness, which are not accounted for by the PE model. Regardless of the explanation, these outliers suggest that, at high frequencies, the uncertainty in transmission loss may be slightly greater than predicted by the model-based analysis.

The maximum deviation of field measurements of transmission loss compared to spherical and cylindrical spreading was 10 dB over the 10 km of range measured. The deviation is expected to increase at longer ranges. We assume a standard deviation of 10 dB out to a few 10s of km in range.

Unlike wave-equation models, geometrical spreading models do not account for the effect of source depth and receiver depth on transmission loss. Because the sea-surface acts as a sound-cancelling boundary, attenuation is considerably greater for sources and receivers close to the sea-surface (less than ¼ wavelength deep). We have accounted for the source-depth effect in the geometrical spreading loss model by including a depth-attenuation correction in the shipping source levels (see Section 2.1.2). Nonetheless, geometrical spreading will tend to overestimate sound levels for receivers within a few metres of the sea-surface, particularly at low frequencies.

4.4. Uncertainty of the Cumulative Noise Map

The predicted received level *RL* is related to the assumed source level *SL* and the modelled transmission loss *TL* via a sonar equation:

$$RL = SL - TL$$

The estimated standard deviation of source level spectra was 7 dB (see Section 4.2.). The standard deviation of transmission loss determined by model comparison to field measurements was estimated as 10 dB over a few 10s of km in range (see Section 4.3.). By means of error propagation, the standard deviation of the received level along any transect out to a few 10s of km in range is thus:

$$\sigma_{RL} = \sqrt{\sigma_{SL}^2 + \sigma_{TL}^2} = 12dB$$

At longer ranges, transmission loss is too great to add significantly to a cumulative noise map.

The error of the cumulative noise level in each cell of the geographic grid depends on the number of neighbouring grid cells that contribute significantly to cumulative energy. The error of the cells with low levels of cumulative noise is larger than the error of cells with high levels of cumulative noise. This is because the cells will low received levels will experience a higher number of significant contributions from neighbouring cells and from cells at longer ranges. The energy in cells that are source cells largely depends on the dominant vessel class (dominant in terms of source power and hours) and is thus a combination of the 7 dB standard deviation in source level and a 5 dB standard deviation in transmission loss over the 1.9 km mean distance within a source cell, resulting in a combined error of ±9 dB.

The received level computed for each source cell was computed as the level received at an average distance of 1.9 km from the cell centre. This is not the distance of mean power. The distance of mean power is shorter than 1.9 km, because of the logarithmic loss of energy with range. The resulting cumulative map therefore gives the received level at average ranges from the source. It does not give the average amount of energy injected into each cell by shipping, even though at long receiver ranges, these amounts approximate each other. A map of average energy injected into the ocean would enhance the shipping lanes compared to Figure 7.

We also note that standard deviations are commonly given in terms of dB in acoustics. Mathematically, this is not strictly correct, as sound level distribution is not Gaussian.

4.5. Fine-Scale Modelling

Figure 7 shows the mean received underwater acoustic energy over one year of shipping in BC waters. The region receiving the most energy includes the Straits of Georgia and Juan de Fuca, and Puget Sound. This is because of the ports of Vancouver and Seattle. A secondary hot spot can be identified around the port of Prince Rupert. In order to resolve BC's narrow straits and fjords, a finer-scale model is needed with a resolution better than the 5 km x 5 km grid used in this study.

Fine-scale modelling is computationally prohibitive over large geographic areas as in the current study. Results of the current study, however, can identify regions that deserve fine-scale investigation.

A fine-scale model could include a more sophisticated hence computationally expensive sound propagation model, such as a full parabolic equation (PE) model. Fine-scale modelling must involve reanalysis of vessel tracks and re-computation of a shipping traffic map at a finer grid resolution. With an average distance of 1.9 km from the centre of a 5 km x 5 km cell, the received level is up to 75 dB below the source level. A finer shipping density grid will resolve the actual ship lanes much better and will also give a more realistic received level closer to the actual lanes.

One method of cumulative modelling on a finer scale over a 20 km x 20 km area was developed by Erbe and King (2009). A finer grid of source and receiver locations was established, sound propagation transects were extracted from the environment and clustered with a neural network. A PE model was run on all cluster centroids, and transmission loss extrapolated for all transects. The increase in computational speed thanks to the neural network was a factor 55. The resulting standard deviation of the error surface was 3 dB based on a comparison of the neural network approach to a full PE solution.

Fine-scale models are powerful for the prediction of noise from proposed, future operations. For example in the case of planned port development, the fine-scale model can compare the current noise from shipping to future increases based on increases in port size and resulting traffic.

4.6. Potential Ecological-Scale Effects

Environmental impact assessments of underwater noise have historically considered single operations (e.g. one oil rig, one pile driving operation for port construction, one seismic survey at a time) and their effects on individual animals or a single population. However, impact should be integrated over time and space. As animals move through their habitat they experience different operations. Impact can be cumulative (Erbe, 2012; Wright, 2012). Our model integrates noise energy over time and space to produce a map of cumulative sound exposure levels. This can be overlain with habitat maps to identify habitats in which animals are at risk from noise exposure, in much the same way that risk assessments have been conducted in BC to identify areas where marine mammals may experience elevated risk of ship strike (Williams and O'Hara, 2010) or entanglement in marine plastics (Williams *et al.*, 2011). If one were to plot animal migration routes, one could integrate the energy a single animal receives over the course of months to a year.

Our model predictions have important implications for conservation and management of resident killer whales, whose legally designated critical habitats include acoustics as a key habitat element (Fisheries and Oceans Canada, 2011). Our models predict that these critical habitat areas (including Haro Strait and Johnstone Strait) are among the noisiest sites within Canada's Pacific EEZ (Figure 7). A skeptic will note that ship energy peaks below 500 Hz for all classes, whereas orca hearing sensitivity peaks at 20 kHz (Szymanski *et al.*, 1999). One of the clearest lessons of the last decade of research on

marine mammals and noise is that an animal's response to noise cannot be predicted from its audiogram. Harbour porpoise are high-frequency hearing specialists, but they avoid habitat exposed to broadband pile-driving noise at ranges beyond 20 km from the source (Tougaard *et al.*, 2009). Killer whales are also responsive to noise at frequencies far lower than the species' 20 kHz peak frequency. Controlled-exposure experiments demonstrated that resident killer whales showed subtle evasive responses to broadband received levels of 108 dB re 1 µPa from a slow, paralleling boat at 100 m, and much more obvious evasive responses to broadband received levels of 116 dB re 1 µPa from a fast, leap-frogging boat at 150 m (Williams *et al.*, 2002a; Williams *et al.*, 2002b).

Our study met its main objective to produce a predicted noise surface that integrates noise sources throughout a year and across a large spatial scale. Future analyses should make an effort to include other sources of noise than large ships. Currently, pile-driving associated with windfarm construction is not a significant contribution of noise in BC waters, but this may change. Similarly, seismic surveys do not currently occur in BC waters, but raise the ambient noise levels in other regions of the world where offshore oil and gas exploration and production is underway. Military sonar introduces transient noise sources that may cause locally important ecological consequences, but is unlikely to raise the average ambient noise profile in this region. The biggest anthropogenic noise source that we have not included in this analysis is propeller noise from boats smaller than those required to call in to MCTS. These boats are unlikely to be captured by AIS sources either. The best way to capture this source is to measure its contribution in a few areas where small-boat traffic is expected to be high.

Our predicted noise surface is suitable for integration into ongoing marine spatial planning exercises in Canada, and our analytical framework can be applied easily in other regions of the world. In Canada, our predictions are immediately applicable for recovery planning for resident killer whales. Next steps would include: field measurements to validate our predictions; fine-scale modelling to resolve noise levels in narrow fjords and passages <10 km in width; identifying potential quiet zones to set aside as acoustic refuges or as experimental control sites to assess ecological impacts of noise on wildlife; and running simulations to predict acoustic consequences of various proposed industrial developments that affect marine traffic in BC. A priority area for additional work is the need to determine whether mainland fjords are several decibels quieter than offshore sites. These sites could have high levels of natural ambient noise that we did not consider, such as more sound from surf or waves. Alternatively, if they really are acoustically isolated from long-distance sources of low-frequency anthropogenic noise, then this may lend itself to area-based management to retain some sites as quiet marine protected areas. At the very least, these small zones could serve as rare and much-needed experimental control sites for the upcoming International Quiet Ocean Experiment (Boyd *et al.*, 2011).

The most important gap in our ability to manage and mitigate impacts of noise on marine wildlife is the need to determine management targets, thresholds or limits of allowable change. We believe strongly that noise should be incorporated into marine spatial planning exercises in Canada, the US and around the world, and our exercise can be viewed as an important step toward a conservation assessment in a systematic conservation planning framework (Margules *et al.*, 2002). But this approach inherently

hinges on having managers specify targets. Canada's Species at Risk Act appears to require agencies to manage human activities to prevent acoustic degradation of critical habitats of resident killer whales, "in order that killer whales can maintain communication, and detect and capture prey while in the area" (Fisheries and Oceans Canada, 2011). These qualitative management objectives have not yet been articulated in terms of quantitative targets.

The United States has formed an Underwater Sound Field Working Group to map underwater noise throughout the waters of the US EEZ. This represents a tremendous step forward in terms of integrating noise into the US commitment to marine spatial planning, but to the best of our knowledge that process has not yet resulted in thresholds identifying allowable change due to cumulative energy from shipping, pile-driving and seismic surveys.

The European Union (EU) has come closer than the US or Canada to defining thresholds. Under the EU Habitats Directive, a Marine Strategy Framework Directive (2008/56/EC) requires that the European Commission specify quantitative criteria and indicators to monitor to allow member states a consistent way to evaluate Good Environmental Status of marine habitats (Tasker *et al.*, 2010). In part, this Directive outlines some specific indicators to monitor for low-frequency, continuous sound:

"The ambient noise level measured by a statistical representative set of observation stations in Regional Seas where noise within the 1/3 octave bands 63 and 125 Hz (centre frequency) should not exceed the baseline values of year [2012] or 100 dB (re 1μPa RMS; average noise level in these octave bands over a year)."

The average sound pressure level from shipping can be estimated from our cumulative sound exposure map (Figure 7) by dividing the energy by the total number of seconds in the year 2008. This is equal to a subtraction of 75 dB from the colour scale in Figure 7. Considering energy only in the two 1/3 octave bands centred at 63 and 125 Hz gives an estimate of ambient levels that are going to be monitored in Europe. Figure 12 shows in pink the regions where the annual average noise level from shipping exceeded the European goal of 100 dB re 1 μPa in either the 63 Hz or 125 Hz 1/3 octave band based on our model.

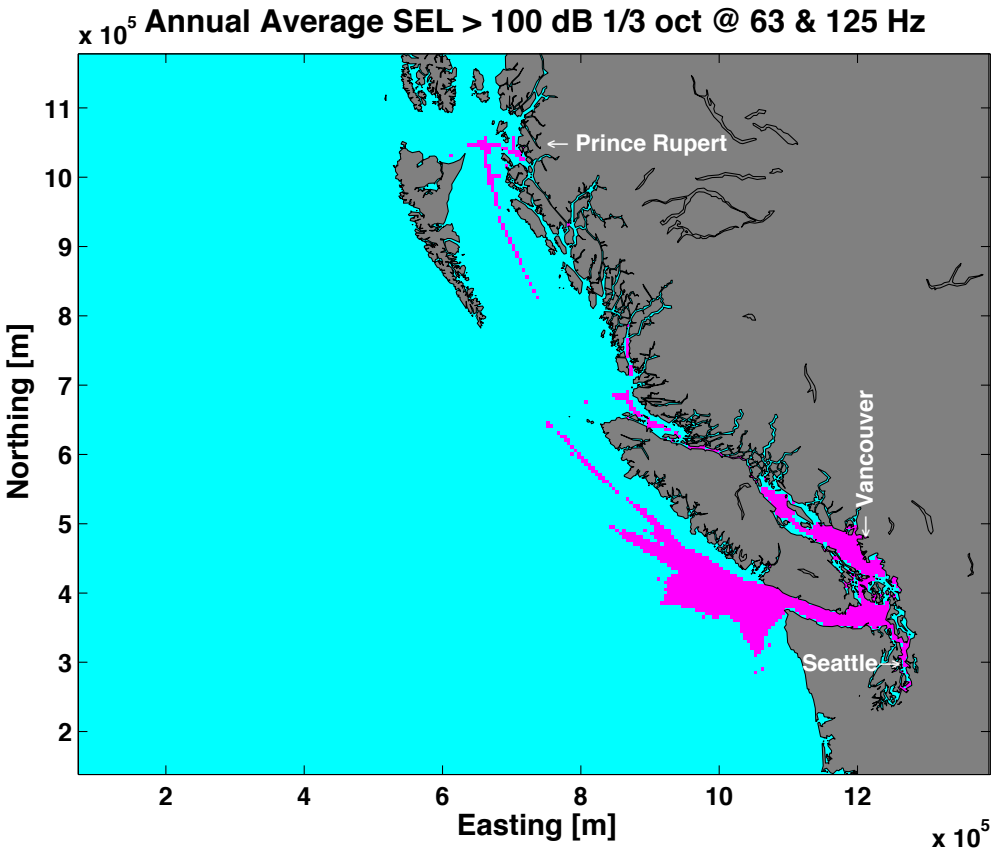

Figure 12: Estimated annual average sound pressure level (RMS) plotted as either exceeding (pink) or not exceeding (blue) the EU Marine Strategy Framework Directive of 100 dB (RMS) in 1/3-octave bands centred at 63 Hz or 125 Hz. Note that much of southern BC waters, including critical habitats for northern and southern resident killer whales, are predicted to exceed a threshold that would warrant closer attention under EU policy. Many mainland inlets, much of Hecate Strait and most of the pelagic parts of Canada's Pacific EEZ are expected to satisfy this criterion for "Good Environmental Status" under the EU Habitats Directive.

4.7. CONCLUSION

In summary, we developed an efficient tool to predict underwater noise from shipping over large areas and long durations. The tool takes vessel logs and propagates sound from all vessel positions through an ocean environment, accumulating acoustic energy over time. While the tools were developed for Canadian Pacific waters, the approach is widely transferable and computationally efficient.

While the model was constructed from data on ship traffic over the year 2008, data from any year can be entered into the model. The tools can thus be used to analyse trends in past and future shipping noise in order to inform marine spatial planning.

Finally, the model predictions have immediate real-world applications in terms of guiding conservation and management. The two places where Canada has a legal obligation to be concerned about high ambient noise levels (namely critical habitats for northern and southern resident killer whales) are predicted to have higher ambient noise levels than other parts of Canada's Pacific EEZ. In fact, killer whale critical habitats in Johnstone and Haro Straits are likely to exceed limits that define "good conservation status" under the EU Marine Strategy Framework Directive. Additional resources are needed to identify whether these model predictions hold true in central and south coast and offshore waters, and if so, to identify ways to reduce the anthropogenic contribution to ambient noise in the region.

Acknowledgement

The ship traffic database was compiled by the Oil-in-Canadian-Waters (OCW) research group consisting of: Dr. Ron Pelot (Dalhousie University), Dr. Patrick O'Hara (EC-CWS), Dr. David Lieske (Mt Allison University), Dr. Rosaline Canessa (University of Victoria), Dr. Stefannia Bertazzon (University of Calgary), and Norma Serra-Sogas (University of Victoria). Dr. Patrick O'Hara was extremely helpful, formatting the database to suit our model, computing vessel speeds in different geographic regions, computing speed and length statistics, and answering numerous questions.

Last but not least, we gratefully acknowledge the support of WWF-Canada.

Disclaimer

The results and recommendations presented in this report do not necessarily represent the official position of WWF-Canada.

5. LITERATURE CITED

American National Standards Institute. (2004). Specification for octave-band and fractional-octave-band analog and digital filters (ANSI S1.11-2004). New York: Acoustical Society of America.

Austin, M., MacGillivray, A., Hannay, D., and Zykov, M. (2010). *Enbridge Northern Gateway Project: Marine Acoustics Technical Data Report (2006)*. Victoria, B.C.: JASCO Applied Sciences.

Baird, R. W., Hanson, M. B., and Dill, L. M. (2005). Factors influencing the diving behaviour of fish- eating killer whales: sex differences and diel and interannual variation in diving rates. *Canadian Journal of Zoology, 83*, 257-267.

Barrie, J. V., and Bornhold, B. (1989). Surficial geology of Hecate Strait, British Columbia contintental shelf. *Canadian Journal of Earth Sciences*(26), 1241–1254.

Barrie, J. V., and Hill, P. R. (2004). Holocene faulting on a tectonic margin: Georgia Basin, British Columbia, Canada. *Geo-Marine Letters, 24*, 86-96.

Barrie, J. V., Luternauer, J. L., Conway, K. W., and Caltagirone, A. (1990). *Surficial geology of the Queen Charlotte Basin*.

Bornhold, B., and Barrie, J. (1991). Surficial sediments on the Western Canadian continental shelf. *Continental Shelf Research, 11*, 685–699.

Boyd, I. L., Frisk, G., Urban, E., Tyack, P., Ausubel, J., Seeyave, S., Cato, D., Southall, B., Weise, M., Andrew, R., Akamatsu, R., Dekeling, R., Erbe, C., Farmer, D. M., Gentry, R., Gross, T., Hawkins, A. D., Li, F. C., Metcalf, K., Miller, J. H., Moretti, D., Rodrigo, C., and Shinke, T. (2011). An International Quiet Oceans Experiment. *Oceanography*.

Breeding, J. E., Pflug, L. A., Bradley, M., Herbert, M., and Wooten, M. (1994). *RANDI 3.1 User's Guide*: Naval Research Laboratory.

Breeding, J. E., Pflug, L. A., Bradley, M., Walrod, M. H., and McBride, W. (1996). *Research Ambient Noise Directionality (RANDI) 3.1 Physics Description*: Planning System Incorporated.

Brekhovskikh, L. M., and Lysanov, Y. P. (2003). *Fundamentals of Ocean Acoustics* (3rd edition ed.). New York: New York.

Buckingham, M. J. (2005). Compressional and shear wave properties of marine sediments: Comparisons between theory and data. *Journal of the Acoustical Society of America, 117*(1), 137-152.

Carnes, M. R. (2009). *Description and evaluation of GDEM-V 3.0*: Naval Research Laboratory.

Clark, C. W., Ellison, W. T., Southall, B. L., Hatch, L., Van Parijs, S. M., Frankel, A., and Ponirakis, D. (2009). Acoustic masking in marine ecosystems: intuitions, analysis, and implication. *Marine Ecology-Progress Series, 395*, 201-222.

Clay, S., and Medwin, H. (1977). *Acoustical Oceanography*. New York: Wiley.

Collins, M. D., Cederberg, R. J., King, D. B., and Chin-Bing, S. (1996). Comparison of algorithms for solving parabolic wave equations. *Journal of the Acoustical Society of America, 100*(1), 178-182.

Cosens, S. E., and Dueck, L. P. (1988). Responses of migrating narwhal and beluga to icebreaker traffic at the Admiralty Inlet ice-edge, N.W.T. in 1986. In W. M. Sackinger & M. O. Jeffries (Eds.), *Port and Ocean Engineering under Arctic Conditions* (pp. 39-54). Fairbanks, Alaska: Geophysical Institute, University of Alaska.

Cosens, S. E., and Dueck, L. P. (1993). Icebreaker noise in Lancaster Sound, N.W.T., Canada: implications for marine mammal behavior. *Marine Mammal Science, 9*(3), 285-300.

D'Amico, A., Gisiner, R., Ketten, D., Hammock, J., Johnson, C., Tyack, P., and Mead, J. (2009). Beaked Whale Strandings and Naval Exercises. *Aquatic Mammals, 35*(4), 452-472.

Deecke, V. B., Ford, J. K. B., and Spong, P. (2000). Dialect change in resident killer whales: implications for vocal learning and cultural transmission. *Animal Behaviour, 60*, 629-638.

Ellison, W., Southall, B., Clark, C., and Frankel, A. (2011). A new context-based approach to assess marine mammal behavioral responses to anthropogenic sounds. *Conservation Biology*.

Erbe, C. (2000). Detection of whale calls in noise: Performance comparison between a beluga whale, human listeners and a neural network. *Journal of the Acoustical Society of America, 108*(1), 297-303.

Erbe, C. (2002). Underwater noise of whale-watching boats and its effects on killer whales (*Orcinus orca*). *Marine Mammal Science, 18*(2), 394-418.

Erbe, C. (2008). Critical ratios of beluga whales (*Delphinapterus leucas*) and masked signal duration. *Journal of the Acoustical Society of America, 124*(4), 2216-2223.

Erbe, C. (2009). Underwater noise from pile driving in Moreton Bay, Qld. *Acoustics Australia, 37*(3), 87-92.

Erbe, C. (2012). The effects of underwater noise on marine mammals. In A. N. Popper & A. D. Hawkins (Eds.), *The Effects of Noise on Aquatic Life. Advances in Experimental Medicine and Biology 730* (pp. 17-22). New York: Springer Verlag.

Erbe, C., and Farmer, D. M. (1998). Masked hearing thresholds of a beluga whale (*Delphinapterus leucas*) in icebreaker noise. *Deep-Sea Research Part II, 45*(7), 1373-1388.

Erbe, C., and Farmer, D. M. (2000a). A software model to estimate zones of impact on marine mammals around anthropogenic noise. *Journal of the Acoustical Society of America, 108*(3), 1327-1331.

Erbe, C., and Farmer, D. M. (2000b). Zones of impact around icebreakers affecting beluga whales in the Beaufort Sea. *Journal of the Acoustical Society of America, 108*(3), 1332-1340.

Erbe, C., King, A., Yedlin, M., and Farmer, D. (1999). Computer models for masked hearing experiments with beluga whales (*Delphinapterus leucas*). *Journal of the Acoustical Society of America, 105*(5), 2967-2978.

Erbe, C., and King, A. R. (2009). Modeling cumulative sound exposure around marine seismic surveys. *Journal of the Acoustical Society of America, 125*(4), 2443-2451.

Finley, K. J., Miller, G. W., Davis, R. A., and Greene, C. R. (1990). Reactions of belugas, Delphinapterus leucas, and narwhals, Monodon monoceros, to ice-breaking ships in the Canadian High Arctic. *Advances in Research on the Beluga Whale, Delphinapterus leucas (Can. Bull. Fish. Aquat. Sci. 224).* 97-117.

Fisheries and Oceans Canada. (2011). *Recovery Strategy for the Northern and Southern Resident Killer Whales (Orcinus orca) in Canada*.

François, R. E., and Garrison, G. R. (1982a). Sound absorption based on ocean measurements: Part I: Pure water and magnesium sulphate contributions. *Journal of the Acoustical Society of America, 72*(3), 896-907.

François, R. E., and Garrison, G. R. (1982b). Sound absorption based on ocean measurements: Part II: Boric acid contribution and equation for total absorption. *Journal of the Acoustical Society of America, 72*(6), 1879-1890.

Halpern, B. S., Walbridge, S., Selkoe, K. A., Kappel, C. V., Micheli, F., D'Agrosa, C., Bruno, J. F., Casey, K. S., Ebert, C., Fox, H. E., Fujita, R., Heinemann, D., Lenihan, H. S., Madin, E. M. P., Perry, M. T., Selig, E. R., Spalding, M., Steneck, R., and Watson, R. (2008). A Global Map of Human Impact on Marine Ecosystems. *Science 319*, 948-952.

Hamilton, E. L. (1980). Geoacoustic modeling of the sea floor. *Journal of the Acoustical Society of America, 68*(5), 1313-1340.

Hatch, L. T., and Fristrup, K. M. (2009). No barrier at the boundaries: implementing regional frameworks for noise management in protected natural areas. *Marine Ecology Progress Series, 395*, 223-244.

Hilliard, R. C., and Pelot, R. (2011). *Traffic data preparation for the Oil In Canadian Waters Project. Maritime Activity and Risk Investigation Network [MARIN]*

Howes, D. E., Zacharias, M. A., and Harper, J. R. (1997). *British Columbia Marine Ecological Classification: Marine Ecosections and Ecounits*.

International Standardization Organization. (1975). International Standard ISO 266-1975 (E): Acoustics--Preferred frequencies for measurements.

MacGillivray, A. O. (2006). *An Acoustic Modelling Study of Seismic Airgun Noise in Queen Charlotte Basin.* M.Sc. Thesis, University of Victoria, B.C.

Margules, C., Pressey, R., and Williams, P. (2002). Representing biodiversity: data and procedures for identifying priority areas for conservation. *Journal of Biosciences, 27*(4), 309-326.

McKenna, M. F., Ross, D., Wiggins, S. M., and Hildebrand, J. A. (2012). Underwater radiated noise from modern commercial ships. *Journal of the Acoustical Society of America, 131*(1), 92-103.

Moilanen, A., Wilson, K. A., and Possingham, H. P. (2009). *Spatial conservation prioritisation: quantitative methods and computational tools*. Oxford: Oxford University Press.

Mooney, T. A., Hanlon, R. T., Christensen-Dalsgaard, J., Madsen, P. T., Ketten, D. R., and Nachtigall, P. E. (2010). Sound detection by the longfin squid (Loligo pealeii) studied with auditory evoked potentials: sensitivity to low-frequency particle motion and not pressure. *Journal of Experimental Biology, 213*(21), 3748-3759.

National Research Council. (2003). *Ocean Noise and Marine Mammals*. New York: National Academies Press.

Purser, J., and Radford, A. N. (2011). Acoustic noise induces attention shifts and reduces foraging performance in three-spined sticklebacks (Gasterosteus aculeatus). *PloS one, 6*(2), e17478.

Richardson, W. J., Greene, C. R., Malme, C. I., and Thomson, D. H. (1995). *Marine Mammals and Noise*. San Diego: Academic Press.

Rolland, R. M., Parks, S. E., Hunt, K. E., Castellote, M., Corkeron, P. J., Nowacek, D. P., Wasser, S. K., and Kraus, S. D. (2012). Evidence that ship noise increases stress in right whales. *Proceedings of the Royal Society B: Biological Sciences*.

Ross, D. (1976). *Mechanics of Underwater Noise*. New York: Pergamon Press.

Scrimger, P., and Heitmeyer, R. M. (1991). Acoustic source-level measurements for a variety of merchant ships. *Journal of the Acoustical Society of America, 89*(2), 691-699.

Simpson, S. D., Meekan, M., Montgomery, J., McCauley, R., and Jeffs, A. (2005). Homeward Sound. *Science, 308*, 221.

Simpson, S. D., Radford, A. N., Tickle, E. J., Meekan, M. G., and Jeffs, A. G. (2011). Adaptive Avoidance of Reef Noise. *Plos One, 6*(2), -.

Szymanski, M. D., Bain, D. E., Kiehl, K., Pennington, S., Wong, S., and Henry, K. R. (1999). Killer whale (Orcinus orca) hearing: Auditory brainstem response and behavioral audiograms. *Journal of the Acoustical Society of America, 106*(2), 1134-1141.

Tasker, M. L., Amundin, M., Andre, M., Hawkins, A. D., Lang, W., Merck, T., Scholik-Schlomer, A., Teilman, J., Thomsen, F., Werner, S., and Zakharia, M. (2010). *Marine Strategy Framework Directive: Task Group 11 Report: Underwater noise and other forms of energy* (JRC Scientific and Technical Report No. EUR 24341 EN - 2010). Luxembourg: European Commission and International Council for the Exploration of the Sea.

Tougaard, J., Carstensen, J., and Teilmann, J. (2009). Pile driving zone of responsiveness extends beyond 20 km for harbor porpoises (Phocoena phocoena (L.)) (L). *Journal of the Acoustical Society of America, 126*(1), 11-14.

Tyack, P. L. (2008). Implications for marine mammals of large-scale changes in the marine acoustic environment. *Journal of Mammalogy, 89*(3), 549-558.

Tyack, P. L., and Clark, C. W. (2000). Communication and acoustic behavior of dolphins and whales. In W. W. L. Au, A. N. Popper & R. R. Fay (Eds.), *Hearing by Whales and Dolphins* (pp. 156-224). New York: Springer-Verlag.

Urick, R. J. (1983). *Principles of Underwater Sound* (3rd ed.). New York: McGraw Hill.

Vermeij, M. J. A., Marhaver, K. L., Huijubers, C., Nagelkerken, I., and Simpson, S. D. (2010). Coral Larvae Move toward Reef Sounds. *PloS ONE, 5*(5), 1-4.

Wagstaff, R. A. (1973). *RANDI: Research Ambient Noise Directionality Model*. San Diego, CA: Naval Ship Systems Command.

Wales, S. C., and Heitmeyer, R. M. (2002). An ensemble source spectra model for merchant ship-radiated noise. *The Journal of the Acoustical Society of America, 111*(3), 1211-1231.

Williams, R., Ashe, E., and O'Hara, P. D. (2011). Marine mammals and debris in coastal waters of British Columbia, Canada. *Marine Pollution Bulletin, 62*(6), 1303-1316.

Williams, R., Bain, D. E., Ford, J. K. B., and Trites, A. W. (2002a). Behavioral responses of male killer whales to a "leapfrogging" vessel. *Journal of Cetacean Research and Management, 4*, 305-310.

Williams, R., Lusseau, D., and Hammond, P. S. (2006). Estimating relative energetic costs of human disturbance to killer whales (Orcinus orca). [doi: 10.1016/j.biocon.2006.06.010]. *Biological Conservation, 133*(3), 301-311.

Williams, R., and O'Hara, P. (2010). Modelling ship strike risk to fin, humpback and killer whales in British Columbia, Canada. *Journal of Cetacean Research and Management, 11*(1), 1-8.

Williams, R., Trites, A. W., and Bain, D. E. (2002b). Behavioural responses of killer whales (*Orcinus orca*) to whale-watching boats: opportunistic observations and experimental approaches. *Journal of Zoology, 256*, 255-270.

Wilson, B., and Dill, L. M. (2002). Pacific herring respond to simulated odontocete echolocation sounds. *Canadian Journal of Fisheries and Aquatic Sciences, 59*(3), 542-553.

Wright, A. J. (2012). Noise-related stress and cumulative impact assessment. In A. N. Popper & A. D. Hawkins (Eds.), *The Effects of Noise on Aquatic Life. Advances in Experimental Medicine and Biology 730* (pp. 541-544). New York: Springer Verlag.

Zhang, Y., and Tindle, C. (1995). Improved equivalent fluid approximations for a low shear speed ocean bottom. *Journal of the Acoustical Society of America, 98*(6), 3391-3396.

6. GLOSSARY

6.1. PRESSURE

Hydrostatic pressure at any given depth in a *static* liquid is the result of the weight of the liquid acting on a unit area at that depth, plus any pressure acting on the surface of the liquid.

Acoustic pressure is a deviation from the ambient hydrostatic pressure caused by a sound wave.

Pressure is measured with a *microphone* in air, and a *hydrophone* under water.

The common symbol and units are: P [1 bar = 10^5 Pa = 10^6 dyn/cm^2].

A recorded pressure time series is symbolised as $P(t)$, with t symbolising time.

PEAK SOUND PRESSURE

Peak pressure is the maximum absolute value of the amplitude of a pressure time series $P(t)$. It is also called the zero-to-peak amplitude.

PEAK SOUND PRESSURE LEVEL

The peak pressure level (SPL_{Pk}) is the logarithmic ratio of peak pressure to reference pressure:

$$SPL_{Pk} = 20\log_{10}\left(\max(|P(t)|/P_{ref})\right)$$

The *peak pressure level* is expressed in *decibels*: dB re 1 µPa. The *reference pressure* underwater is P_{ref} = 1 µPa.

PEAK-TO-PEAK PRESSURE LEVEL

The *peak-to-peak pressure level* ($SPL_{Pk\text{-}Pk}$) is the difference (expressed in decibels) between the maximum and the minimum of the recorded pressure time series [dB re 1 µPa].

$$SPL_{Pk-Pk} = 20\log_{10}\left(\left(\max(P(t)) - \min(P(t))\right)/P_{ref}\right)$$

RMS SOUND PRESSURE

The *rms sound pressure* is the root-mean-square of the time series $P(t)$. This quantity is useful for continuous sound (as opposed to pulsed).

RMS SOUND PRESSURE LEVEL

The *rms sound pressure level* (SPL_{rms}) is the logarithmic ratio of *rms* pressure to reference pressure [dB re 1 µPa]:

$$SPL_{rms} = 20\log_{10}\left(\sqrt{\frac{1}{T}\int_T P(t)^2\,dt}\,/\,P_{ref}\right)$$

For pulsed sound such as from airguns or pile driving, the *SPLrms* level depends on the duration *T* over which the pressure is averaged. This duration would ideally be the pulse duration. However, it is difficult to determine the pulse start and end times. Pulse duration is therefore taken as the time between the 5% and the 95% points on the cumulative energy curve. *SPLrms* is computed by averaging the squared pressure over the time window between $T_{5\%}$ and $T_{95\%}$.

6.2. Power Spectral Density

Power spectral density describes how the power of a signal is distributed with frequency. For a received signal in the far field, the mean square pressure spectral density is the contribution to mean square pressure per Hertz.

Power Spectral Density Level

The p*ower or mean square pressure spectral density level* is computed as $10\log_{10}$ of the mean square pressure in 1-Hz bands [dB re 1 µPa²/Hz].

Spectral Density Percentiles

Percentile plots show how sound varies over time. The n^{th} percentile gives the level that is exceeded n% of the time (note: in engineering, the definition is reversed). The 50^{th} percentile corresponds to the median.

6.3. Sound Exposure Level

The *sound exposure level* (SEL) is a measure of the total *energy* of a signal over the duration *T* [dB re 1 µPa²•s]. For plane waves,

$$SEL = 10\log_{10}\left(\int_T P(t)^2\, dt\right)$$

In the presence of significant ambient noise $P_n(t)$, noise energy needs to be subtracted to compute *sound exposure* from the signal alone. In practise, the noise energy is computed from a time section preceding or succeeding the signal:

$$SEL = 10\log_{10}\left(\int_0^T P(t)^2\, dt - \int_{Tn}^{Tn+T} P_n(t)^2\, dt\right)$$

6.4. Source Level

The acoustic *source level* is the level referenced to a distance of 1 m from a point source. For sources that are physically larger than a few cm (ship propellers and drillrigs for example), the spectrum is measured at some range, and a sound propagation model applied to compute what the spectrum would have been at 1 m range if the source could have been collapsed into a point-source. In other words, the source level is a measure of the amount of sound in the far field, and therefore its measurement has to be made in the far field.

The *source level* can be expressed in terms of pressure [dB re 1 µPa at 1 m] or sound exposure [dB re 1 µPa²s at 1 m].

6.5. 1/3 Octave Band Levels

The energy of a sound split into a series of adjacent frequency bands, each being 1/3 of an octave wide. The centre frequencies f_C of adjacent 1/3 octave bands are computed as $f_C(n) = 10^{n/10}$, where n counts the 1/3 octave bands.

Table 6: Centre frequencies of adjacent 1/3 octave bands [Hz](American National Standards Institute, 2004; International Standardization Organization, 1975)

10	12.5	16
20	25	31.5
40	50	63
80	100	125
160	200	250
315	400	500
630	800	1000
1250	1600	2000
2500	3150	4000
5000	6300	8000
10000	12500	16000
20000	25000	31500

6.6. Sound Speed Profile

A graph of the speed of sound in the water column as a function of depth.

7. APPENDIX: NOISE LAYERS BY VESSEL CLASS

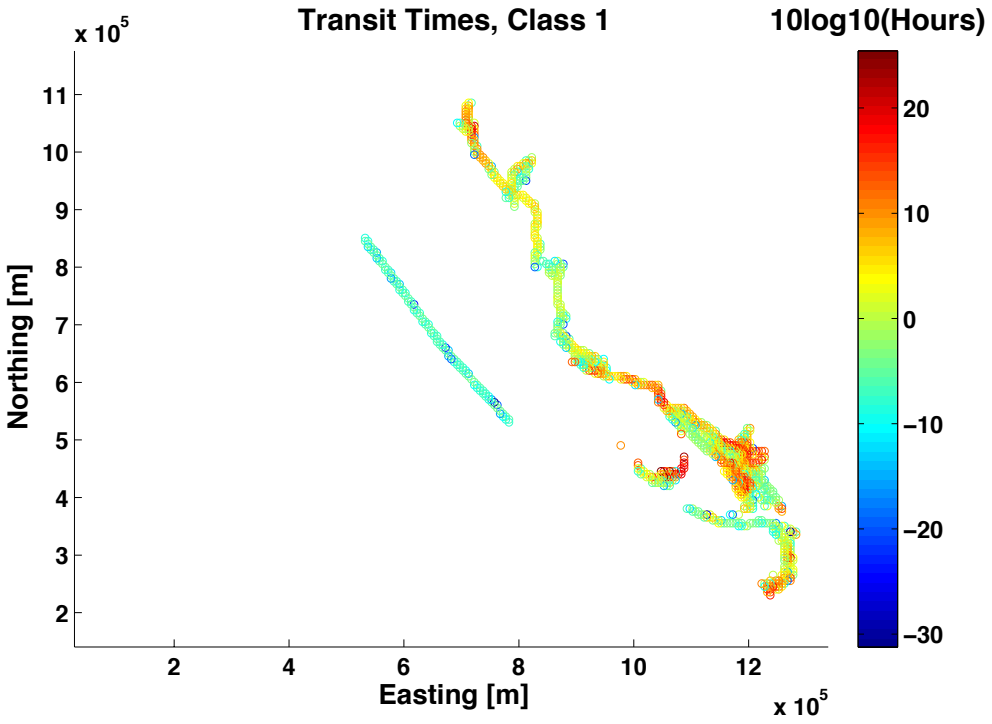

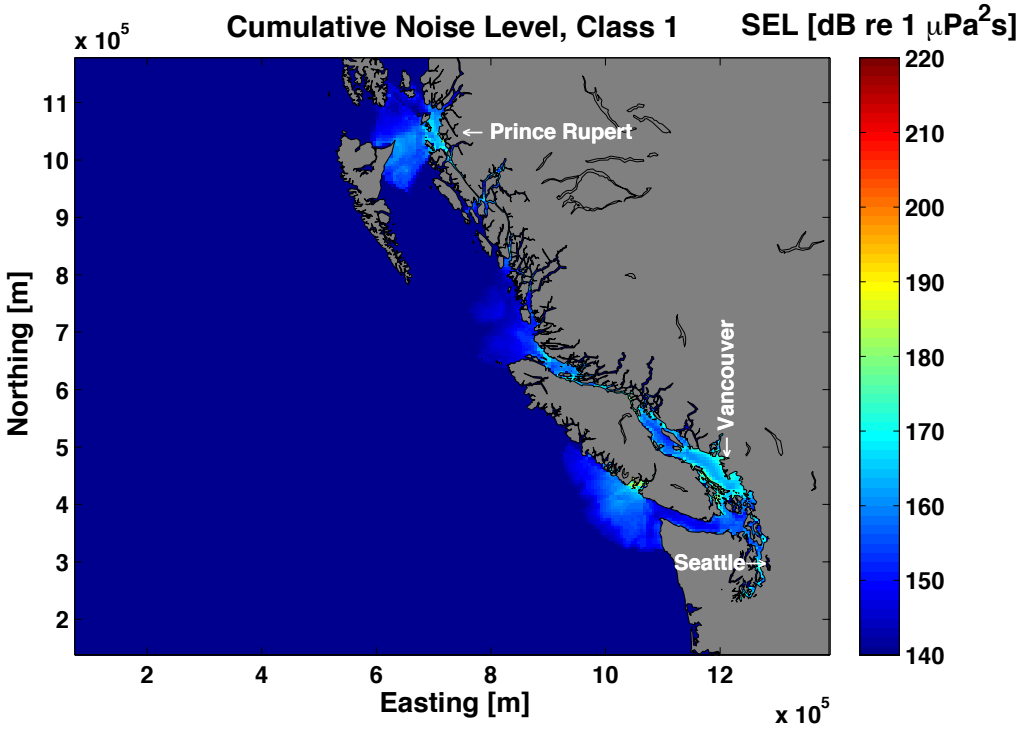

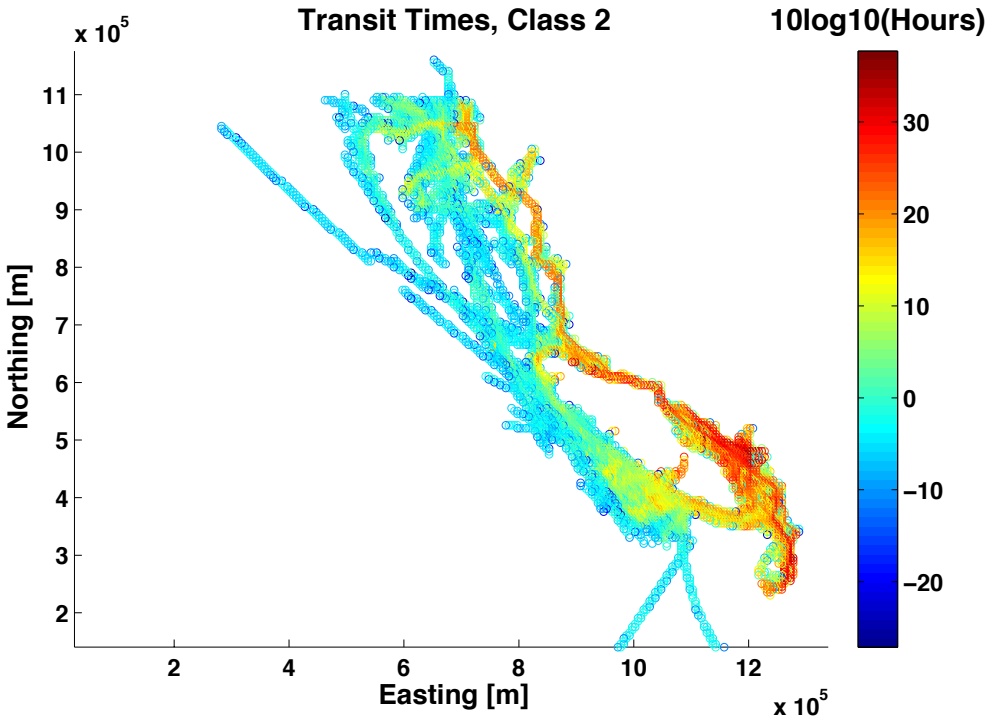
Transit Times, Class 2
10log10(Hours)
x 10^5
Northing [m]
Easting [m]
x 10^5
11
10
9
8
7
6
5
4
3
2
2
4
6
8
10
12
30
20
10
0
−10
−20

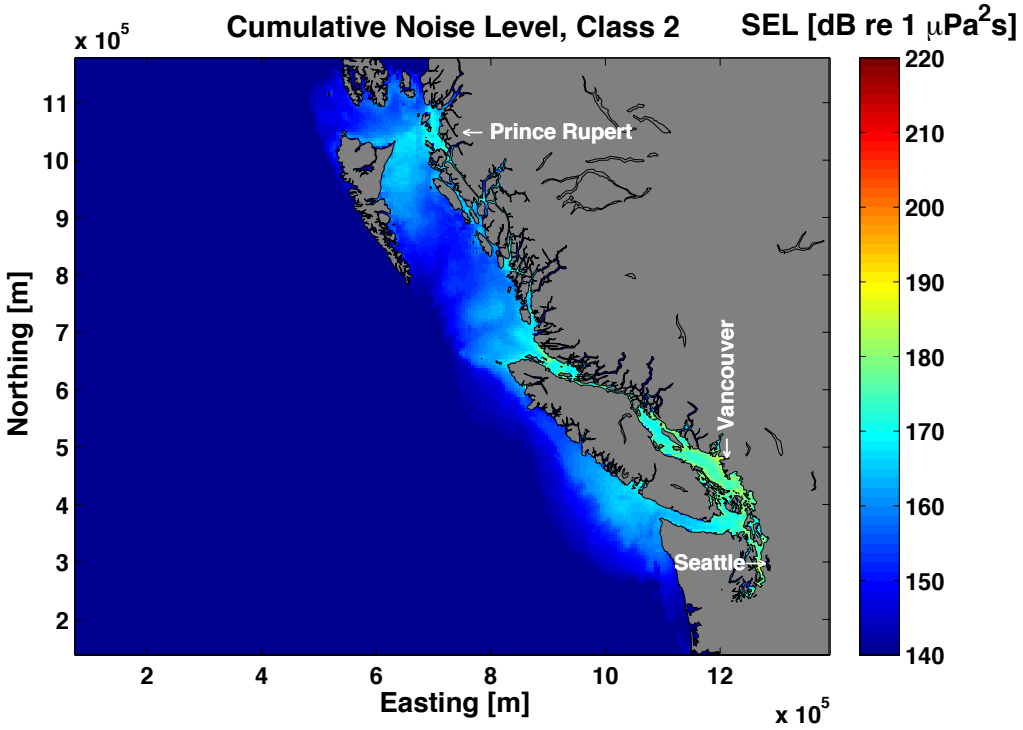
Cumulative Noise Level, Class 2
SEL [dB re 1 μPa²s]
x 10^5
Northing [m]
Easting [m]
x 10^5
← Prince Rupert
← Vancouver
Seattle →
11
10
9
8
7
6
5
4
3
2
2
4
6
8
10
12
220
210
200
190
180
170
160
150
140

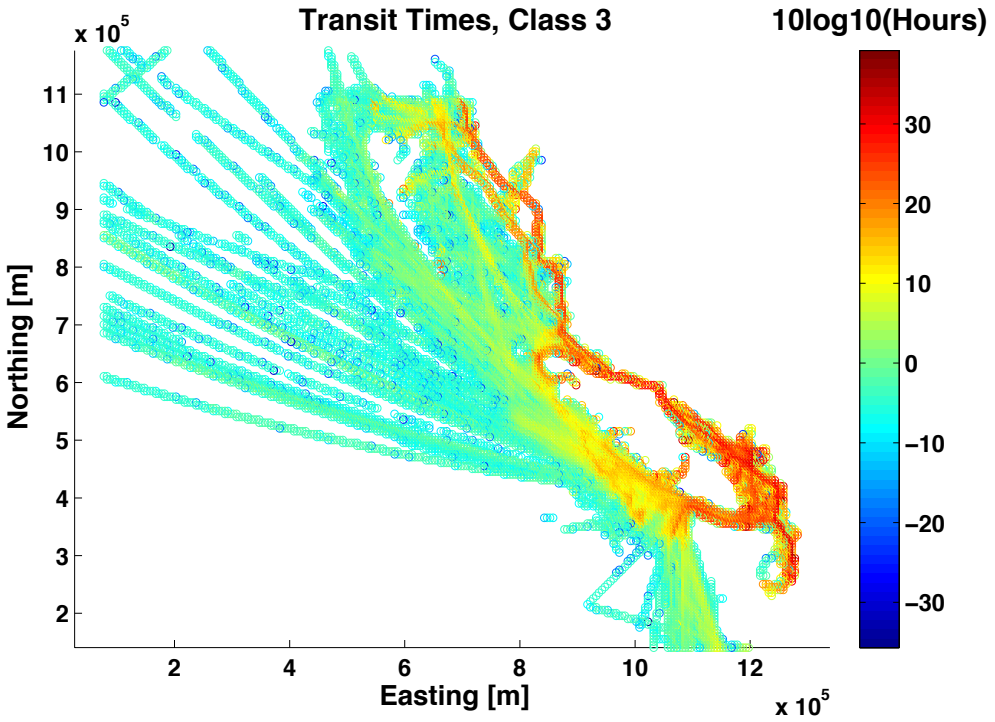
Transit Times, Class 3
10log10(Hours)
x 10^5
Northing [m]
Easting [m]
x 10^5
11
10
9
8
7
6
5
4
3
2
2
4
6
8
10
12
30
20
10
0
−10
−20
−30

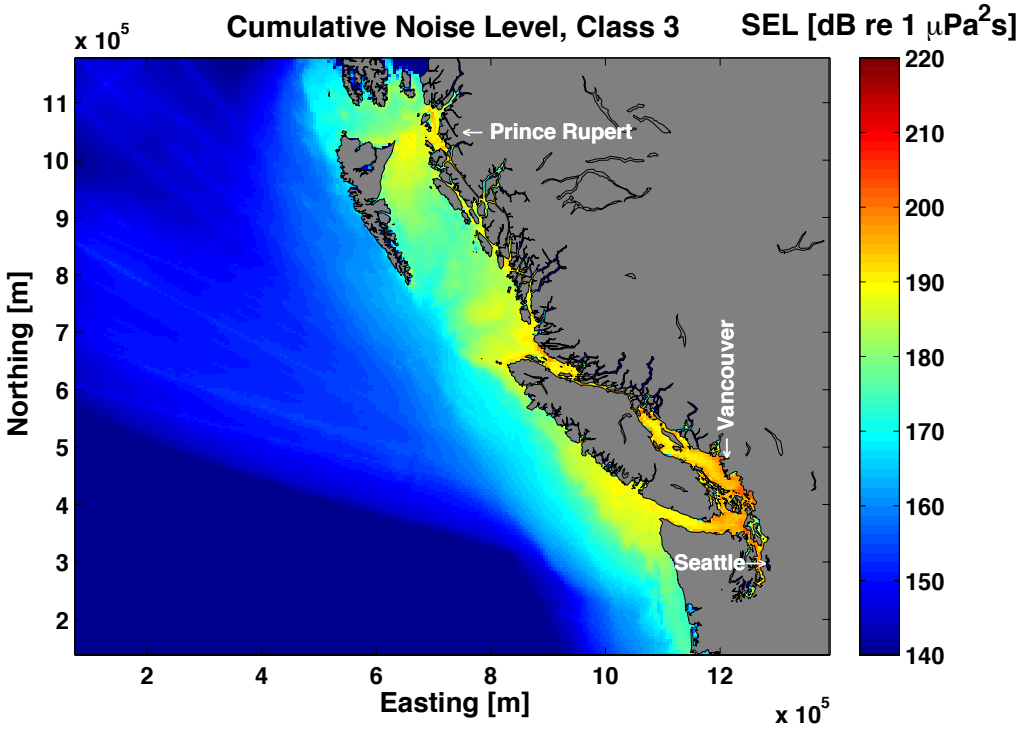
Cumulative Noise Level, Class 3
SEL [dB re 1 μPa²s]
x 10^5
Northing [m]
Easting [m]
x 10^5
← Prince Rupert
← Vancouver
Seattle →
11
10
9
8
7
6
5
4
3
2
2
4
6
8
10
12
220
210
200
190
180
170
160
150
140

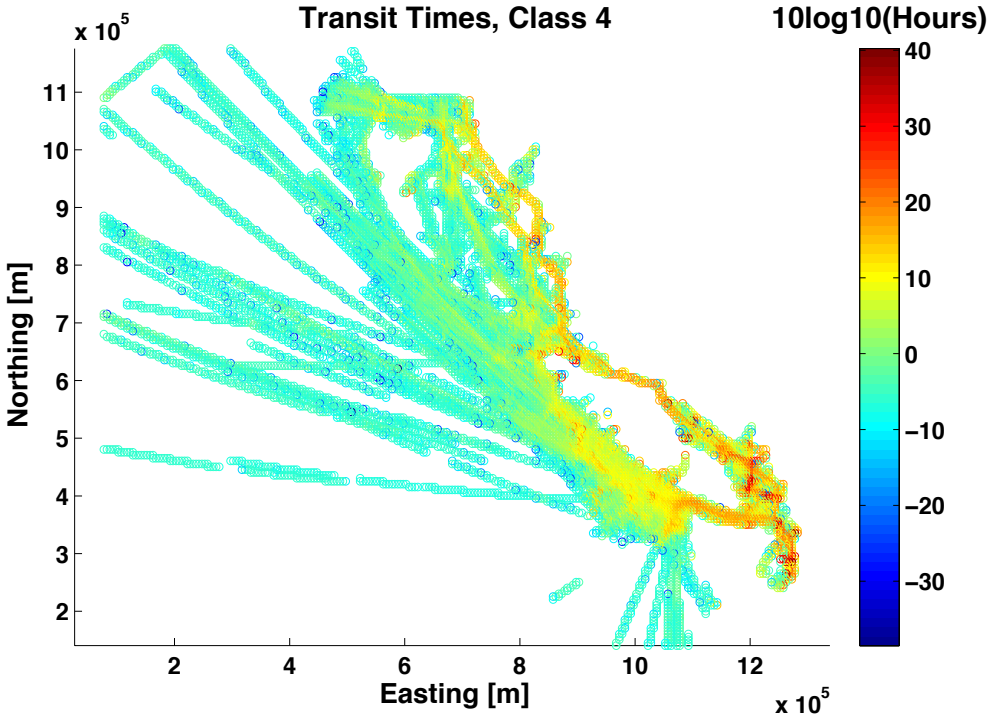
Transit Times, Class 4
10log10(Hours)
x 10^5
Northing [m]
Easting [m]
x 10^5
40
30
20
10
0
−10
−20
−30

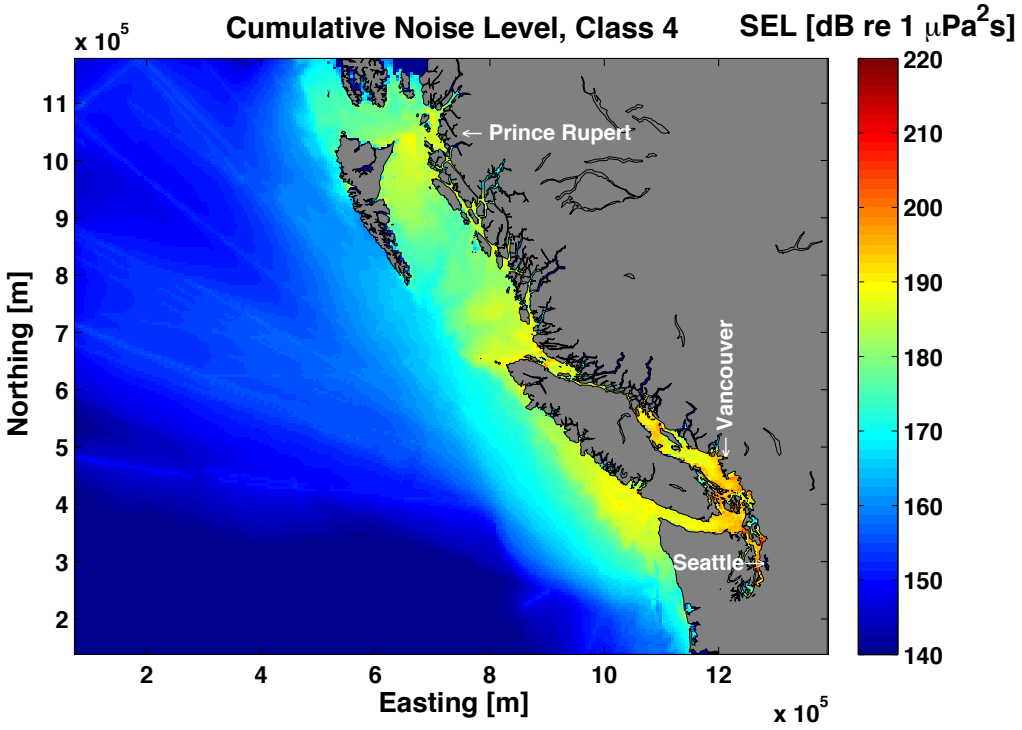
Cumulative Noise Level, Class 4
SEL [dB re 1 μPa²s]
x 10^5
Prince Rupert
Vancouver
Seattle
Northing [m]
Easting [m]
x 10^5
220
210
200
190
180
170
160
150
140

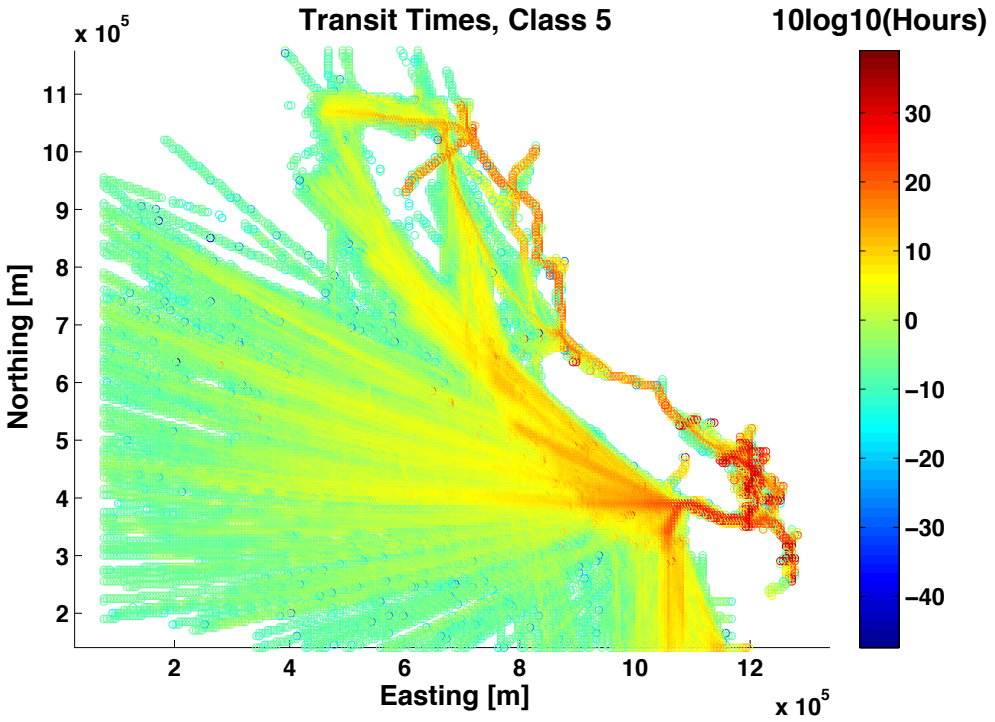
Transit Times, Class 5
10log10(Hours)
x 10^5
Northing [m]
Easting [m]
x 10^5
11
10
9
8
7
6
5
4
3
2
2
4
6
8
10
12
30
20
10
0
−10
−20
−30
−40

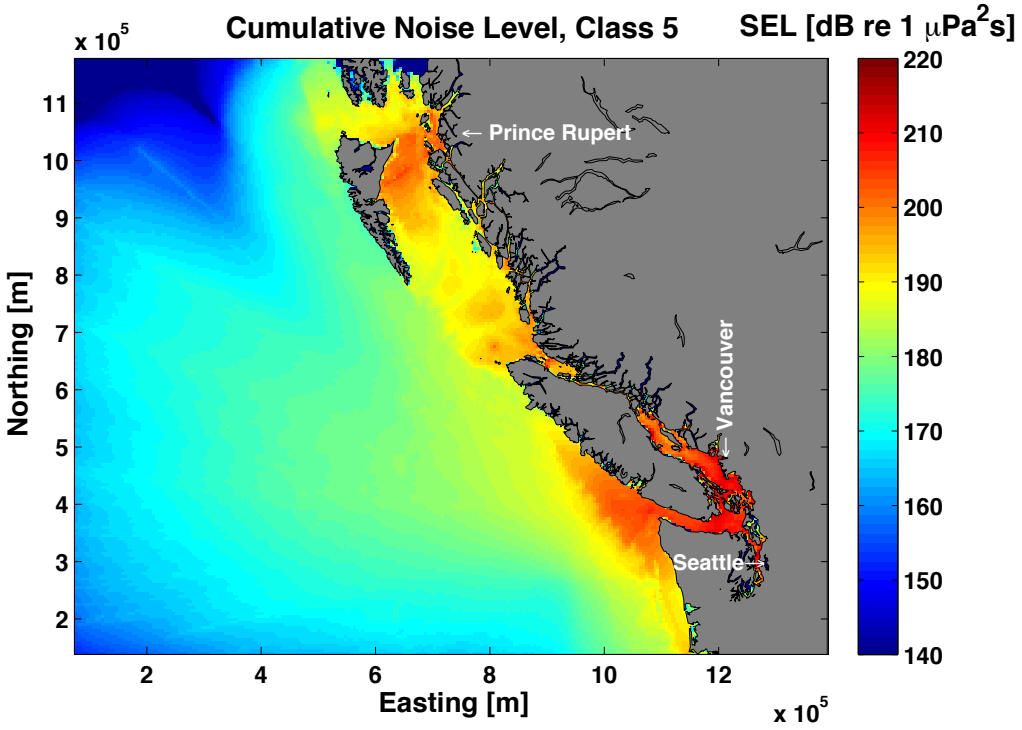
Cumulative Noise Level, Class 5
SEL [dB re 1 μPa²s]
x 10^5
Northing [m]
Easting [m]
x 10^5
← Prince Rupert
Vancouver →
Seattle →
11
10
9
8
7
6
5
4
3
2
2
4
6
8
10
12
220
210
200
190
180
170
160
150
140

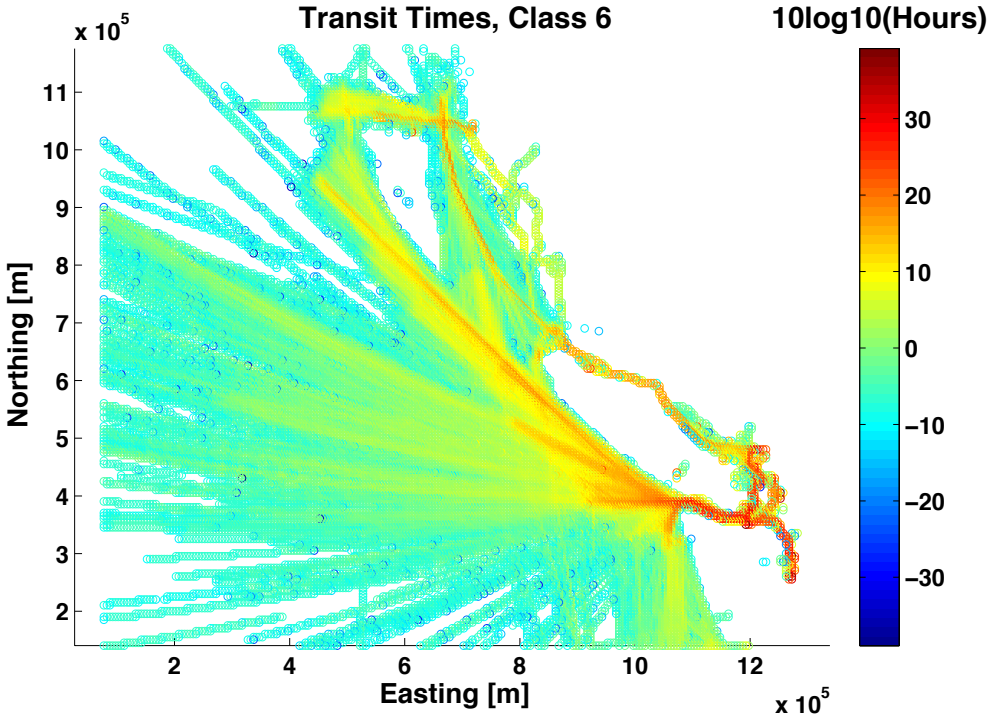
Transit Times, Class 6
10log10(Hours)
x 10^5
Northing [m]
Easting [m]
x 10^5
11
10
9
8
7
6
5
4
3
2
2
4
6
8
10
12
30
20
10
0
−10
−20
−30

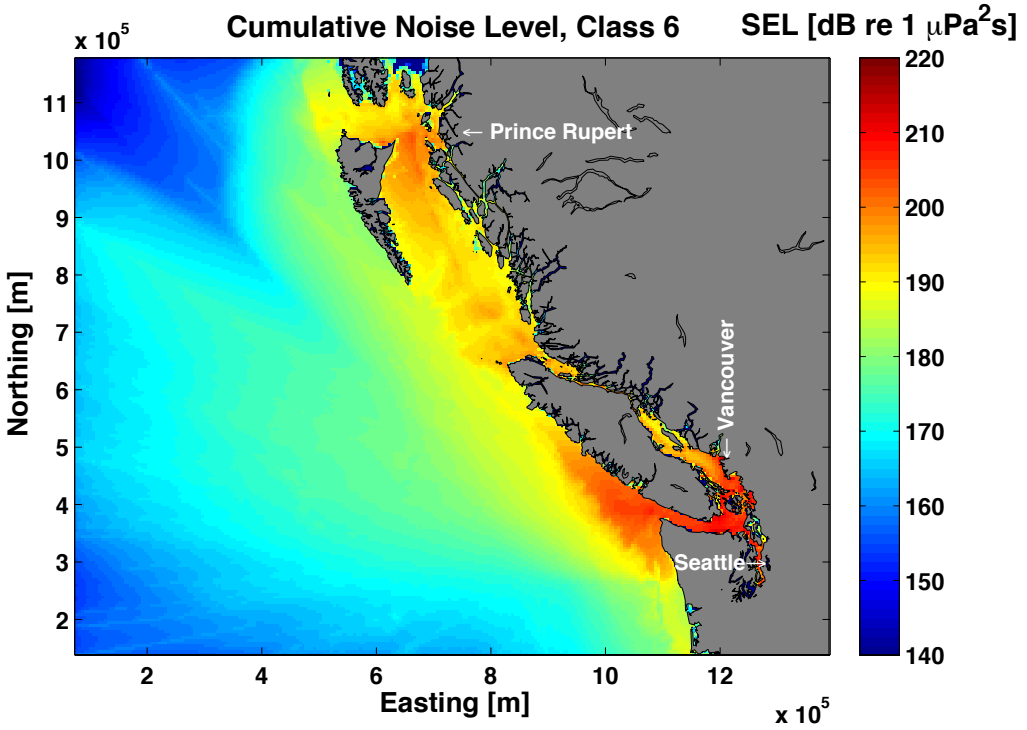
Cumulative Noise Level, Class 6
SEL [dB re 1 μPa²s]
x 10^5
Northing [m]
Easting [m]
x 10^5
← Prince Rupert
← Vancouver
Seattle →
11
10
9
8
7
6
5
4
3
2
2
4
6
8
10
12
220
210
200
190
180
170
160
150
140

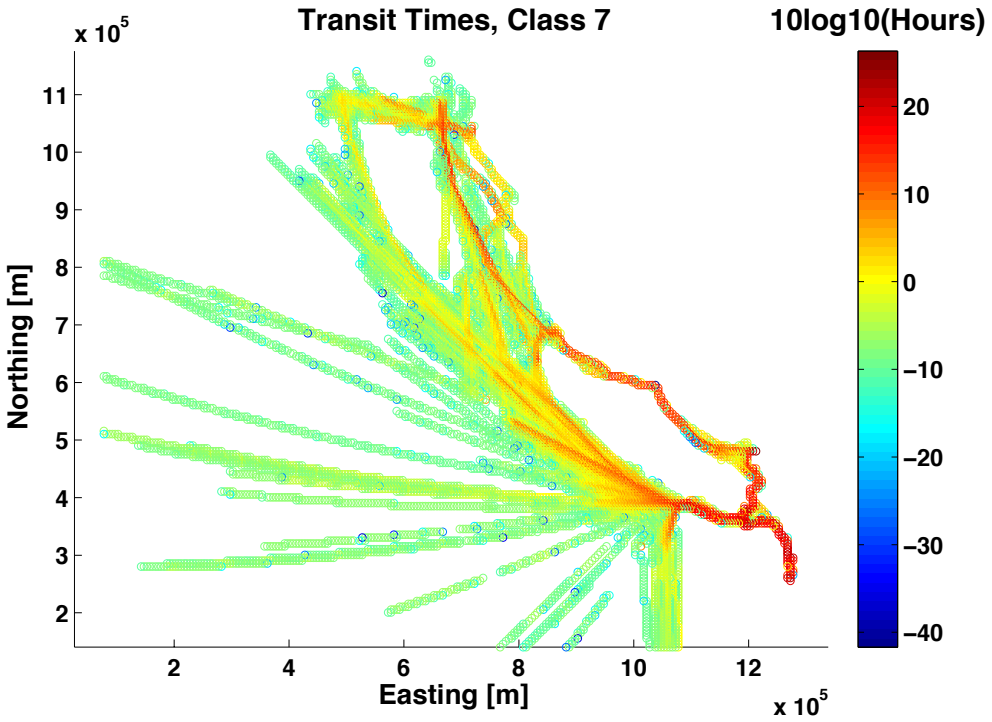
Transit Times, Class 7
10log10(Hours)
x 10^5
Northing [m]
Easting [m]
x 10^5
11
10
9
8
7
6
5
4
3
2
2
4
6
8
10
12
20
10
0
−10
−20
−30
−40

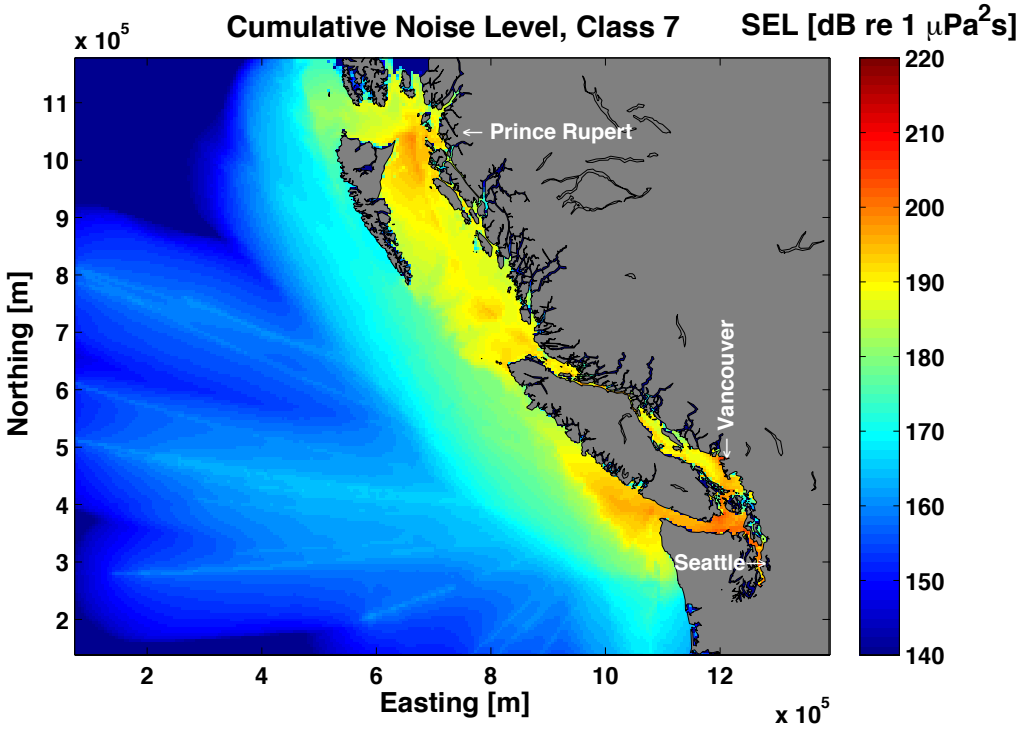
Cumulative Noise Level, Class 7
SEL [dB re 1 μPa²s]
x 10^5
Northing [m]
Easting [m]
x 10^5
← Prince Rupert
← Vancouver
Seattle →
11
10
9
8
7
6
5
4
3
2
2
4
6
8
10
12
220
210
200
190
180
170
160
150
140